Design, Synthesis, in Vitro and in Vivo Biological Evaluation of 2-Amino-3-Aroylbenzo[*b*]furan Derivatives as Highly Potent Tubulin Polymerization Inhibitors

Paola Oliva,[a] Romeo Romagnoli,[a]* Stefano Manfredini,[b] Andrea Brancale,[c] Salvatore Ferla,[c] Ernest Hamel,[d] Roberto Ronca,[e] Federica Maccarinelli,[e] Arianna Giacomini,[e] Fatlum Rruga,[f] Elena Mariotto,[f] Giampietro Viola,[f,g]* Roberta Bortolozzi [f]*

[a]Dipartimento di Scienze Chimiche e Farmaceutiche, Università degli Studi di Ferrara, Via Luigi Borsari 46, 44121 Ferrara, Italy;

[b]Department of Life Sciences and Biotechnology, University of Ferrara, Via Fossato di Mortara 17-19, 44121 Ferrara, Italy;

[c]School of Pharmacy and Pharmaceutical Sciences, Cardiff University, King Edward VII Avenue, Cardiff, CF10 3NB, UK;

[d]Screening Technologies Branch, Developmental Therapeutics Program, Division of Cancer Treatment and Diagnosis, Frederick National Laboratory for Cancer Research, National Cancer Institute, National Institutes of Health, Frederick, Maryland 21702, USA;

[e]Dipartimento di Medicina Molecolare e Traslazionale Unità di Oncologia Sperimentale ed Immunologia, Università di Brescia, 25123 Brescia, Italy;

[f]Dipartimento di Salute della Donna e del Bambino, Laboratorio di Oncoematologia, Università di Padova, 35131 Padova, Italy;

[g]Istituto di Ricerca Pediatrica (IRP), Corso Stati Uniti 4, 35128 Padova, Italy.

* To whom correspondence should be addressed. Phone: 39-(0)532-455303. Fax: 39-(0)532-455953. E-mail: rmr@unife.it (R.R.); Phone: 39-(0)49-8211451. Fax: 39-(0)49-8211462. E-mail: giampietro.viola1@unipd.it (G.V.). Phone: 39-(0)49-8215485 E-mail:

roberta.bortolozzi@unipd.it (R.B.).

Abstract: A new class of inhibitors of tubulin polymerization based on the 2-amino-3-(3',4',5'-trimethoxybenzoyl)benzo[*b*]furan molecular scaffold was synthesized and evaluated for *in vivo* and *in vitro* biological activity. These derivatives were synthesized with different electron-releasing or electron-withdrawing substituents at one of the C-4 through C-7 positions. Methoxy substitution and location on the benzene part of the benzo[*b*]furan ring played an important role in affecting antiproliferative activity, with the greatest activity occurring with the methoxy group at the C-6 position, the least with the substituent at C-4. The same effect was also observed with ethoxy, methyl or bromine at the C-6 position of the benzo[*b*]furan skeleton, with the 6-ethoxy-2-amino-3-(3',4',5'-trimethoxybenzoyl)benzo[*b*]furan derivative **4f** as the most promising compound of the series. This compound showed remarkable antiproliferative activity (IC_{50}: 5 pM) against the Daoy medulloblastoma cell line, and **4f** was nearly devoid of toxicity on healthy human lymphocytes and astrocytes. The potent antiproliferative activity of **4f** was derived from its inhibition of tubulin polymerization by binding to the colchicine site. The compound was also examined for *in vivo* activity, showing higher potency at 15 mg/kg compared with the reference compound combretastatin A-4 phosphate at 30 mg/kg against a syngeneic murine mammary tumor.

Keywords. Microtubules, benzo[*b*]furan, *in vivo* activity, inhibition tubulin assembly, colchicine binding site.

1. Introduction

Microtubules, as key components of the cytoskeleton, are dynamic cellular structures in neoplastic and non-neoplastic cells generated by the polymerization of α,β-tubulin heterodimers [1, 2]. The microtubule system of eukaryotic cells is a critical element involved in a variety of essential cellular processes in addition to mitotic spindle assembly. These include determination and maintenance of cell shape, regulation of motility, cell signaling, secretion and intracellular transport [3, 4]. Due to the essential role of microtubules in mitosis and cell division, tubulin is the target for numerous small natural and synthetic molecules that inhibit the formation of the mitotic spindle [5-7]. More recent studies have demonstrated that several small molecules able to interfere with the dynamic assembly of tubulin in generating the microtubule system are also able to induce extensive morphological changes in the endothelial cells of tumor vasculature. Such agents can thus also be classified as vascular disrupting agents [8-10].

Among the natural microtubule depolymerizing agents, combretastatin A-4 (CA-4, **1a;** Figure 1) is one of the more studied compounds. CA-4, isolated from the bark of the South African tree *Combretum caffrum* [11], strongly inhibits the polymerization of tubulin by binding to the colchicine site [12]. CA-4 inhibits cell growth at low to mid-nanomolar concentrations [13]. The water soluble sodium phosphate prodrug of CA-4 (CA-4P, fosbretabulin or Zybrestat, **1b**) is actually in phase III clinical trials for the treatment of anaplastic thyroid cancer and Phase II trials for non-small-cell lung cancer [14, 15], while the related serine aminoacid prodrug of 3'-amino-deoxycombretastatin A-4 (Ombrabulin or AVE8062, **1c**) was found to have more potent activity compared with CA-4P and is in phase I clinical studies for patients with solid tumors [16]. In addition, CA-4P and AVE8062 demonstrate strong suppressive activity on tumor blood flow, leading to tumor necrosis [17, 18].

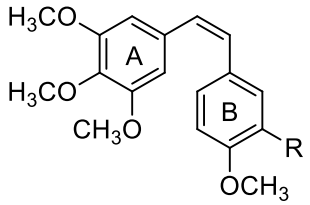

1

R=OH, Combretastatin A-4 (CA-4), **1a**
R=OPO_3Na_2, CA-4P, **1b**
R=NH-Ser, Ombrabulin (AVE8062), **1c**

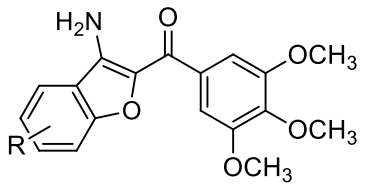

2

R=H or OMe
R=6-OCH_3, **2a**

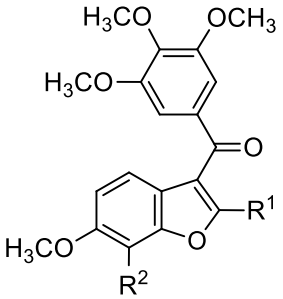

3

R^1=H, Br, CN, CO_2CH_3, alkyl, alkylamine, aryl, heteroaryl
R^2=H or OH
3a, R^1=4'-OMe-3'-OH-C_6H_3, R^2=OH
3b, R^1=CH_3, R^2=OH
3c, R^1=NH_2, R^2=OH

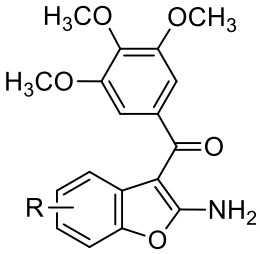

4

R=H, electron-withdrawing (F and Br) or electron-releasing groups such as alkoxy (OCH_3, OC_2H_5, n-OC_3H_7, $OCH_2C_6H_5$), CH_3, OH and NH_2

Figure 1. Representative tubulin depolymerizing agents (CA-4, CA-4P and AVE8062) and general structures **2-4** of inhibitors of tubulin assembly with the benzo[*b*]furan pharmacophore.

Anticancer therapy based on microtubule-targeting agents that bind to tubulin at the colchicine site and disrupt microtubule dynamics have received considerable attention, and there is still a need to identify novel molecules that target microtubules [19-22].

Although many synthetic tubulin inhibitors have been synthesized, among such compounds there are limited examples of chemically diverse small molecule antimitotic agents based on the benzo[*b*]furan molecular skeleton as the core structure [23-30]. During our continuing search directed at the preparation of new small molecule tubulin inhibitors, we previously

reported the discovery of a series of methoxy-substituted 2-(3',4',5'-trimethoxybenzoyl)-3-aminobenzo[*b*]furan derivatives with general structure **2**, as a new class of antimitotic agents [26]. In this series of compounds, potent activity was highly dependent upon the presence and position of four methoxy substituents. In addition to the trimethoxyphenyl ring, a fairly dramatic difference was observed between C-4/5 and C-6/7-methoxy substituted compounds. The greatest activity occurred when the fourth methoxy group was located at the 6- or 7-position, while 4- and 5-methoxy derivatives were inactive. Among the synthesized compounds, derivative **2a**, characterized by the presence of a methoxy group at the 6-position of the benzo[*b*]furan skeleton, displayed the greatest antiproliferative activity with IC_{50} values ranging from 87 to 430 nM against a panel of four different cancer cell lines. This agent inhibited tubulin polymerization by binding to the colchicine site on tubulin (IC_{50}: 1.1 μM for assembly) and caused G2/M phase arrest of the cell cycle.

The 3-(3',4',5'-trimethoxybenzoyl)-6-methoxybenzo[*b*]furan molecular skeleton was the core structure of a series of agents with general structure **3** identified by Flynn and co-workers as potent inhibitors of both tubulin polymerization and cell proliferation of the MCF-7 human breast cancer cell line [29, 30]. While at the C-2 position there was a wide tolerance to structural variation with hydrophobic and hydrophilic substituents, at the C-3 position the carbon linker with the 3',4',5'-trimethoxyphenyl substituent was more effective as a carbonyl group than as a carbinol or a simple methylene group [29]. Previous studies have shown that the concomitant presence of a C-6 methoxy substituent significantly contributed to maximize activity, presumably as a mimic of the 4-methoxy group in the B-ring of CA-4 [29]. The introduction of a hydroxyl at the C-7 position was well tolerated and afforded compounds with similar potency as with R^2=H, while a 10-fold increase in activity was observed with R^2=OH [30]. Among the synthesized compounds, the C-2 3'-hydroxy-4'-methoxyphenyl analogue **3a** showed potent activity in inhibiting the growth of the MCF-7 cell line (IC_{50}: 4

nM), with a significant effect on inhibition of tubulin polymerization (IC_{50}: 0.8 μM). Replacement of C-2 aryl group with a methyl furnished derivative **3b** (BNC105), a potent and selective antiproliferative (IC_{50}: 3 nM on MCF-7 cells) and antitubulin (IC_{50}: 3 μM for tubulin assembly) agent, which causes strong tumor vasculature disruption and exhibits tumor growth inhibitory properties in xenograft tumor models [30, 31]. These data confirmed that the 4-methoxy-3-hydroxy groups in the B-ring of CA-4 correlates with the 6-methoxy-7-hydroxy substituents on the benzene portion of the benzo[*b*]furan skeleton.

Compound **3c**, obtained by replacing the C-2 methyl group of **3b** with an amino moiety, was characterized by a 2-amino-3-(3',4',5'-trimethoxybenzoy)benzo[*b*]furan skeleton and can be also considered as a positional isomer of compounds with general structure **2**, switching the position of the amino and 3',4',5'-trimethoxybenzoyl groups. Compound **3c** was able to inhibit the growth of activated and quiescent human umbilical vein endothelial cells (HUVECs), with a selectivity ratio of 4.6, but neither its antiproliferative activity on cancer cell lines nor its inhibition of tubulin assembly was reported [30]. This compound has been re-synthesized by a facile and rapid chemical approach reported here, resulting in a compound equipotent with CA-4 as an inhibitor of tubulin assembly (IC_{50}: 0.59 μM). By comparing activity as inhibitors of tubulin polymerization of **3c** to **3a** and **3b**, the amino moiety of **3c** can be considered a good surrogate for the 4'-methoxy-3'-hydroxyphenyl ring or methyl group present at the 2-position of 3-(3',4',5'-trimethoxybenzoy)benzo[*b*]furan system of compounds **3a** and **3b**. We can presume that the presence of the amino group at the C-2 position of the benzo[*b*]furan system should be important in restricting the conformation of the adjacent trimethoxybenzoyl moiety into the favored orientation for binding to tubulin by the formation an intramolecular hydrogen bond between one of the hydrogens of the amino group with the carbonyl oxygen of the adjacent trimethoxybenzoyl function.

The biological evaluation of compound **3c** prompted us to continue our research on this class of compounds, extending the structure-activity analysis around compound **3c** in an effort to determine if its activity was maintained, or even improved, by the synthesis of a new series of derivatives with general structure **4**. We developed a new synthetic approach that incorporated the structural motif of the 2-amino-3-(3',4',5'-trimethoxybenzoy)benzo[*b*]furan molecular scaffold, and a series of compounds was synthesized with modifications with respect to positions C-4 to C-7 with substituents with different chemical properties. These substituents included electron releasing moieties, such as alkoxy (methoxy, ethoxy, *n*-propoxy and benzyloxy) methyl, amino and hydroxy, or electron-withdrawing fluorine and bromine groups.

Since the C-6 methoxy moiety proved to be favorable for bioactivity, we evaluated the effect of replacing the strong electron-releasing methoxy with the corresponding ethoxy and *n*-propoxy homologues and by the weaker electron-releasing methyl group, which was well-tolerated in a series of CA-4 analogues [32]. In an effort to design compounds with improved polarity, we also replaced the methoxy group at the C-5 and C-6 position of the benzo[*b*]furan ring with the more hydrophilic amino and hydroxyl moieties, respectively. The presence of an amino group at the C-6 position should be detrimental for activity, as observed in a series of 2-(3',4',5'-trimethoxybenzoyl)benzo[*b*]furan derivatives previously published by us [28]. Also, in a series of 2-(3',4',5'-trimethoxybenzoyl)-3-aminoindoles previously published, the introduction of the electron-withdrawing chloro atom at the C-6 position reduced antiproliferative activity of the resulting compound [33]. For these reasons, molecules characterized by the presence of a chlorine atom or the amino group at the C-6 position of 2-amino-3-(3',4',5'-trimethoxybenzoyl)benzo[*b*]furan system were not prepared.

2. Chemistry

Compounds **4a-n** and **3c** were prepared by an efficient, previously described two-step procedure for the synthesis of 2-amino-3-aroyl benzo[*b*]furans (Scheme 1) [34]. α-Azido chalcones **6a-n** were synthesized via a Knoevenagel condensation reaction of salicylaldehydes **5a-n** [35-37] with 2-azido-1-(3,4,5-trimethoxyphenyl)ethanone [38] in the presence of one equivalent of piperidinium acetate [34]. A solution of α-azido chalcones **6a-n** in CH_3CN was transformed in good yields (60-80%) to the corresponding 2-amino-3-(3',4',5'-trimethoxybenzoyl)benzo[*b*]furan **4a-l**, **7a** and **3c** by heating at reflux in the presence of a catalytic amount (0.2 equiv., 20 mol %) of *p*-toluensulfonic acid (*p*-TSA) for 12 h.

Scheme 1. Synthesis of 2-amino-3-(3',4',5'-trimethoxybenzoyl)benzo[*b*]furan derivatives **4a-n** and **3c**

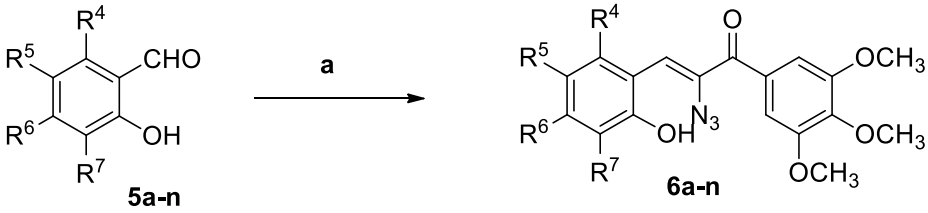

5a-n **6a-n**

5-6a, R^{4-7}=H
5-6b, R^4=OCH_3, R^{5-7}=H
5-6c, R^5=OCH_3, $R^{4,6,7}$=H
5-6d, R^6=OCH_3, $R^{4,5,7}$=H
5-6e, R^7=OCH_3, R^{4-6}=H
5-6f, R^6=OC_2H_5, $R^{4,5,7}$=H
5-6g, R^6=*n*-OC_3H_7, $R^{4,5,7}$=H
5-6h, R^7=OC_2H_5, R^{4-6}=H
5-6i, R^6=$OCH_2C_6H_5$, $R^{4,5,7}$=H
5-6j, R^6=F, $R^{4,5,7}$=H
5-6k, R^6=Br, $R^{4,5,7}$=H
5-6l R^6=CH_3, $R^{4,5,7}$=H
5-6m, R^5=NO_2, $R^{4,6,7}$=H
5-6n, R^6=OCH_3, R^7=OH, $R^{4,5}$=H

b or **c**

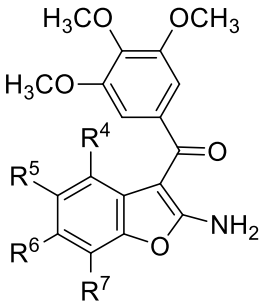

3c, 4a-l and **7a**

4a, R^{4-7}=H
4b, R^4=OCH_3, R^{5-7}=H
4c, R^5=OCH_3, $R^{4,6,7}$=H
4d, R^6=OCH_3, $R^{4,5,7}$=H
4e, R^7=OCH_3, R_{4-6}=H
4f, R^6=OC_2H_5, $R^{4,5,7}$=H
4g, R^6=*n*-OC_3H_7, $R^{4,5,7}$=H
4h, R^7=OC_2H_5, R^{4-6}=H
4i, R^6=$OCH_2C_6H_5$, $R^{4,5,7}$=H
4j, R^6=F, $R^{4,5,7}$=H
4k, R^6=Br, $R^{4,5,7}$=H
4l R^6=CH_3, $R^{4,5,7}$=H
7a, R^5=NO_2, $R^{4,6,7}$=H
3c, R^6=OCH_3, R^7=OH, $R^{4,5}$=H

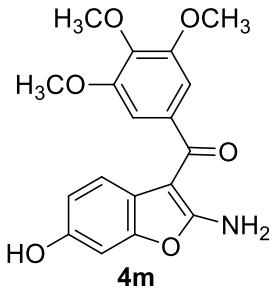

4m

d

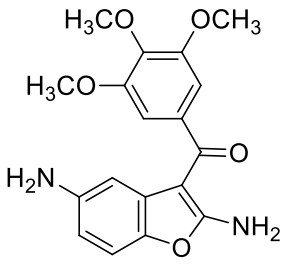

4n

e

Reagents. a: 2-azido-1-(3,4,5-trimethoxyphenyl)ethanone, piperidinium acetate, MeOH, rt, 24 h; **b**: *p*-TSA (0.2 equiv., 20 mol %), CH_3CN, reflux, 12 h; **c**: white CFL (25 W), *p*-TSA (0.2 equiv., 20 mol %), CH_3CN, rt, 24 h, **d**: 10% Pd/C, EtOH, 40 bar, 60 °C, 30 min; **e**: Fe, NH_4Cl, EtOH-H_2O, reflux, 3 h.

The same compounds can also be obtained with a 20-40% reduced yield by a photochemical process replacing the thermal heating with irradiation for 24 h at room temperature with a 25 W white compact fluorescent lamp (CFL). The 6-hydroxy benzo[*b*]furan derivative **4m** was obtained by cleavage of the 6-benzyloxy group of **4i** performed by flow hydrogenolysis with H-Cube® over 10% Pd/C catalyst. 5-Amino benzo[*b*]furan derivative **4n** was generated from the corresponding nitro analogue **7a** by reduction with iron and ammonium chloride in a refluxing mixture of water and ethanol.

3. Biological Results and Discussion

3.1. In vitro antiproliferative activities.

Table 1 summarizes the growth inhibitory effects of 2-amino-3-(3',4',5'-trimethoxybenzoyl)benzo[*b*]furan derivatives **4a-n** and **3c** against a panel of six human cell lines derived from different cancer types. These were cervix carcinoma (HeLa), colon adenocarcinoma (HT-29), medulloblastoma (Daoy), promyelocytic leukemia (HL-60), B-cell leukemia (SEM) and T-cell leukemia (Jurkat). We used the isomeric 6-methoxy-2-(3',4',5'-trimethoxybenzoyl)-3-aminobenzo[*b*]furan derivative **2a** and CA-4 (**1a**) as reference compounds. Nine compounds, including the two reference compounds **2a** and CA-4, had average IC_{50} values below 50 nM (**4c**, **4d**, **4f**, **4g**, **4k**, **4l**, **3c**, **2a** and CA-4), and, for seven of these compounds, the average IC_{50} was below 5 nM (all except **4c** and **4g**). Also, especially notable was the 5 pM IC_{50} value obtained with **4f** against the Daoy medulloblastoma cell line.

Table 1. *In vitro* cell growth inhibitory effects of compounds CA-4 (**1a**), **2a**, **3c** and **4a-n**.

	IC_{50} [a](nM)					
Compd	HeLa	HT-29	Daoy	HL-60	SEM	Jurkat
4a	413±40.3	591±29	371±19	339±21	250±28	385±52
4b	5225±312	6512±263	3950±236	4891±445	4557±369	2760±156
4c	56.0±19	62.9±12.9	36.2±6.9	36.2±11	38.9±12	29.2±9.3
4d	2.9±0.3	5.6±0.9	0.30±0.08	3.0±0.2	4.1±0.2	2.7±0.6
4e	496±39	477±42	345±36	233±31	285±26	333±42
4f	2.8±0.3	2.1±0.2	0.005±0.001	2.7±0.2	0.31±0.05	0.28±0.08
4g	22.7±1.8	17.7±1.2	4.4±0.9	41.7±15.9	29.7±8.9	27.2±1.9
4h	1250±98	910±58	1670±87	428±36	385±27	390±39
4i	9670±125	8680±458	>10000	7056±659	3675±298	4390±154
4j	591±26	682±45	846±28	413±56	333±45	299±39
4k	4.5±0.5	5.4±0.3	2.5±0.2	5.6±0.9	3.5±0.1	2.8±0.6
4l	1.1±0.2	0.6±0.02	0.34±0.1	3.5±0.4	0.30±0.03	0.33±0.05
4m	591±63	3420±368	428±45	285±2.5	371±1.5	299±37
4n	635±1.5	790±98	494±56	413±3.8	259±1.8	399±58
2a	6.2±4.0	787±45	5.0±1.2	3.5±0.3	3.6±0.2	3.1±0.9
3c	15.3±1.9	424±36	0.32±0.06	2.8±0.3	259±19	0.34±0.07
1a	4±1	3100±100	12.3±0.9	1±0.2	5±0.1	0.8±0.2

[a]IC_{50}= compound concentration required to inhibit tumor cell proliferation by 50%. Data are expressed as the mean ± SEM from the dose-response curves of at least three independent experiments.

Derivatives with a methoxy (**4d**), an ethoxy (**4f**), a bromine (**4k**) or a methyl (**4l**) at the C-6 position of the benzo[*b*]furan system exhibited the greatest activity among the tested compounds, with IC_{50} values of 0.30-5.6, 0.005-2.8, 2.5-5.6 and 0.3-3.5 nM, respectively, with compound **4f** having remarkable activity (IC_{50}: 5 pM) against Daoy cells as compared with the other cancer cell lines. None of the synthesized compounds was more active than CA-4 against HL-60 cells, while only derivatives **4f** and **4l** were more potent than CA-4

against HeLa, HT-29, Daoy, SEM and Jurkat cells. The latter three cancer cell lines were highly sensitive to compounds **4f** and **4l**, with IC_{50} values ranging from 0.005 to 0.38 nM. Also, derivatives **4d**, **4l** and **3c** were active at subnanomolar concentrations against Daoy cells, and **3c** was similarly potent (IC_{50}: 0.34 nM) against Jurkat cells.

Comparing the two C-6 methoxy derivatives **2a** and **4d**, the latter being obtained by switching the position of the amino and 3',4',5'-trimethoxybenzoyl moieties at the 2- and 3-positions of the benzo[*b*]furan ring, both compounds were equipotent against HL-60, SEM and Jurkat cells, but **4d** was 2-, 17- and 140-fold more active than **2a** against HeLa, Daoy and HT-29 cells, respectively.

Derivative **4a**, which was unsubstituted in the benzene portion of the benzo[*b*]furan ring, was active at submicromolar concentrations (IC_{50}: 0.25-0.59 μM), and thus less active than derivatives **4c** and **4d** with a methoxy group at the C-5 or C-6 position, respectively, but equipotent with the C-7 methoxy derivative **4e** and more active than the C-4 methoxy analogue **4b**.

In the series of methoxy substituted benzo[*b*]furan derivatives **4b-e**, the data show that potent cancer cell growth inhibition is strongly dependent on the position of the methoxy group. A substantial difference was observed between C-4/7 and C-5/6 substituted compounds (**4b** and **4e** versus **4c** and **4d**). The greatest activity occurred with the methoxy group located at the C-5 or C-6 position, the least when located at the C-4 or C-7 position, with the order being 6-OMe (**4d**)>5-OMe (**4c**)>7-OMe (**4e**)>>4-OMe (**4b**). Thus, compound **4b**, with a methoxy group at the C-4 position, showed modest antiproliferative activity (IC_{50}: 2.8-8.5 μM) and was the least active compound in this series of methoxylated derivatives. Simply moving the methoxy group from the C-4 to the C-5 position (**4c**) resulted in 100-150-fold increased activity, with IC_{50} values ranging from 29 to 56 nM. Activity was further increased 10-120-fold by shifting the methoxy group from the C-5 to C-6 position (**4d**), with the greatest

difference being observed with the Daoy cells (IC_{50}: 36.2 and 0.3 nM for **4c** and **4d**, respectively). Moving the methoxy group to the C-7 position (**4e**) resulted in activity decreasing 2-3-orders of magnitude relative to **4d**, with IC_{50} values ranging from 0.2 to 0.5 μM. The substitution of the C-5 methoxy group of **4c** with an amino group (**4n**) was detrimental to activity, with compound **4n** being 7- to 15-fold less potent than **4d**.

We found that replacement of the C-6 methoxy of **4d** with its ethoxy homologue, to furnish compound **4f**, maintained activity against HeLa and HL-60 cells, and activity was improved 2.5-60-fold against the other four cancer cell lines relative to **4d**, with the difference in activity most pronounced (60-fold) against Daoy cells. Compound **4f** was one of the most potent antiproliferative agents among the newly synthesized compounds, with IC_{50} values of 2.8, 2.1, 0.005, 2.7, 0.31 and 0.28 nM against Hela, HT-29, Daoy, HL-60, SEM and Jurkat cells, respectively. Compound **4f** was 3-fold less active than CA-4 against HL-60 cells (IC_{50}: 2.7 and 1.1 nM, respectively), equipotent to CA-4 against HeLa cells and 3- and 16-fold more active than CA-4 against Jurkat and SEM cells. Enhancement in antiproliferative activity was most evident against Daoy cells (2,460-fold) with **4f**, which was also active against HT-29 cells, which are refractory to CA-4 (IC_{50}: 2.1 nM and 3.1 μM, respectively). Compound **4f** was also considerably superior to its C-7 ethoxy isomer **4h**. A further homologation of the ethoxy group of **4f** to *n*-propoxy (**4g**) reduced antiproliferative activity from one to three orders of magnitude (IC_{50}: 0.005-2.8 and 4.4-41 nM for **4f** and **4g**, respectively), while the C-6 benzyloxy derivative **4i** exhibited no significant antiproliferative activity against the cancer cell lines (IC_{50}: 4-10 μM).

A comparison of the substituent effects revealed that the replacement of the C-6 methoxy with the less electron-releasing methyl group (compounds **4d** and **4l**, respectively) caused a 3-14-fold increased activity against HeLa, HT-29, SEM and Jurkat cells of **4l** relative to **4d**, whereas the methyl and methoxy moieties are interchangeable for activity against Daoy and

HL-60 cells. A drastic loss of activity was observed if the C-6 methoxy group was replaced by the weaker electron-donating and more hydrophilic hydroxy (**4m**) or the electron-withdrawing fluorine (**4j**) moieties. For this latter compound, increasing the size of the halide from fluorine to bromine (**4k**) led to a 71-338-fold increase in activity with all six cell lines, which was most pronounced with the Daoy cells.

The introduction of an additional hydroxyl group at the C-7 position of **4d**, to furnish **3c**, had contrasting effects, with activity being maintained against Daoy and HL-60 cells, while mildly reduced potency relative to **4d** (4-fold) was observed against HeLa cells and more pronounced reduced activity against HT-29 and SEM cells (76- and 63-fold, respectively). Jurkat cells, on the other hand, were 8-fold more sensitive to **3c** than to **4d**.

*3.2. Compounds **4f** and **4l** are non-toxic in non-tumor cells.*

In order to have a preliminary indication of the potential cytotoxicity of these compounds on non-tumor cell lines, the most active compounds, **4f** and **4l**, were evaluated *in vitro* against peripheral blood lymphocytes (PBL) from healthy donors. As shown in Table 2, **4f** had a GI_{50} of 8.7 μM in quiescent lymphocytes. Similarly, in lymphocytes in an active phase of proliferation induced by the mitogenic stimulant phytohematoagglutinin (PHA), the GI_{50} of **4f** was greater than 10 μM. Compound **4l** was similarly inactive, with a GI_{50}>10 μM in both conditions.

Considering that one of the major causes of cytotoxicity of antitubulin drugs is neurotoxicity, we also evaluated the antiproliferative effect of **4f** an **4l** on a line of normal human astrocytes (NHA). Both compounds had a GI_{50} value greater than 10 μM. These initial results suggest that these compounds have very low toxicity in normal cells in comparison to tumor cells, indicating potential for an excellent therapeutic index, perhaps greater than 10.

Table 2. Cytotoxicity of compounds **4f** and **4l** for human PBL and NHA

	GI_{50} (μM) [a]	
Cell line	**4f**	**4l**
$PBL_{resting}$ [b]	8.7±0.7	>10
PBL_{PHA} [c]	>10	>10
NHA	>10	>10

[a] Compound concentration required to inhibit cell growth by 50%.
[b] PBL not stimulated with PHA.
[c] PBL stimulated with PHA.
Values are the mean ± SEM for three separate experiments.

3.3. Inhibition of tubulin polymerization and colchicine binding.

To investigate whether the antiproliferative activities of these compounds were related to interaction with the microtubule system, seven of the most active compounds (**4c-d**, **4f-g**, **4k-l** and **3c**) were evaluated for their inhibition of the polymerization of purified tubulin and inhibition of the binding of [^{3}H]colchicine to tubulin. In the latter assay, the compounds were examined at two different concentrations (5 and 0.5 μM), with tubulin and colchicine at 0.5 and 5 μM concentrations, respectively (Table 3) [39, 40]. For comparison, CA-4 (**1a**) was examined in contemporaneous experiments.

All tested compounds strongly inhibited tubulin assembly, with activities comparable or superior to that of the reference compound CA-4. Compounds **4f** and **4l** seemed to be even more potent than CA-4 (IC_{50}, 0.37, 0.39 and 0.54 μM, respectively), while the others were as active as CA-4 as inhibitors of tubulin assembly, with IC_{50}'s ranging from 0.48 to 0.59 μM. This is in agreement with **4f** and **4l** being the derivatives with the greatest antiproliferative activity.

Table 3. Inhibition of tubulin polymerization and colchicine binding by compounds **4c-d**, **4f-g**, **4k-l**, **3c** and CA-4 (**1a**)

Compound	Tubulin assembly[a] IC_{50}±S.D. (μM)	Colchicine binding[b] % ±S.D.	
		5 μM drug	0.5 μM drug
4c	0.50±0.09	73±0.5	ND
4d	0.48±0.05	99±0.2	79±1
4f	0.37±0.02	99±0.3	86±0.8
4g	0.51±0.1	91±0.3	42±0.4
4k	0.57±0.04	92±1	56±2
4l	0.39±0.04	97±0.4	74±0.1
3c	0.59±0.08	99±1	87±5
CA-4 (**1a**)	0.54±0.06	97±0.8	82±2

ND= not determined

[a] Inhibition of tubulin polymerization. Tubulin was at 10 μM.

[b] Inhibition of [^{3}H]colchicine binding. Tubulin and colchicine were at 0.5 and 5 μM, respectively.

In the colchicine binding studies, all tested compounds potently inhibited the binding of [^{3}H]colchicine to tubulin, with six of them (the exception was **4c**) being as potent as CA-4, when these agents and radiolabeled colchicine were equimolar (5 μM each) in the reaction mixture. However, only derivatives **4d**, **4f, 4l** and **3c** were comparable to CA-4 as inhibitors of colchicine binding when present at one-tenth the concentration of colchicine in the reaction mixture. These data suggested that tested compounds are potent antiproliferative and antitubulin agents acting as microtubule depolymerizing agents through the colchicine site on tubulin.

3.4. Molecular modeling studies.

The potential interaction between these novel 2-amino-3-(3',4',5'-trimethoxybenzoyl)benzo[*b*]furan derivatives and the colchicine site was investigated through molecular docking studies, using Glide [41].

The proposed binding mode for all the new active derivatives is consistent with that of the co-crystallized colchicine, with the trimethoxyphenyl ring in proximity to βCys241, a key interaction point for tubulin polymerization inhibition (Figure 2A). The free amino group at the 2-position of the benzo[*b*]furan ring interacts with αAsn101, potentially locking the compounds in this favorable binding conformation. The benzofuran ring overlaps with the co-crystallized colchicine central core, placing the different substituents at the C-6 position in a small hydrophobic sub-pocket near βMet259, where the colchicine methoxy group is positioned. This small sub-pocket, accommodating the different substituents at the 6-position, can function as an important anchor point, stabilizing the protein-ligand interaction and potentially resulting in a better inhibition of tubulin assembly and antiproliferative activity. In support of this observation, it should be noted that the compounds without a substituent at this position (e.g., **4a**) have reduced antiproliferative activity. No plausible docking poses were found for the almost inactive C-6 benzyloxy derivative **4i** (Figure 2B), as the large benzyl group in the C-6 position cannot be accommodated in the sub-pocket. This observation rationalizes the loss of antiproliferative activity observed for this compound.

A **B**

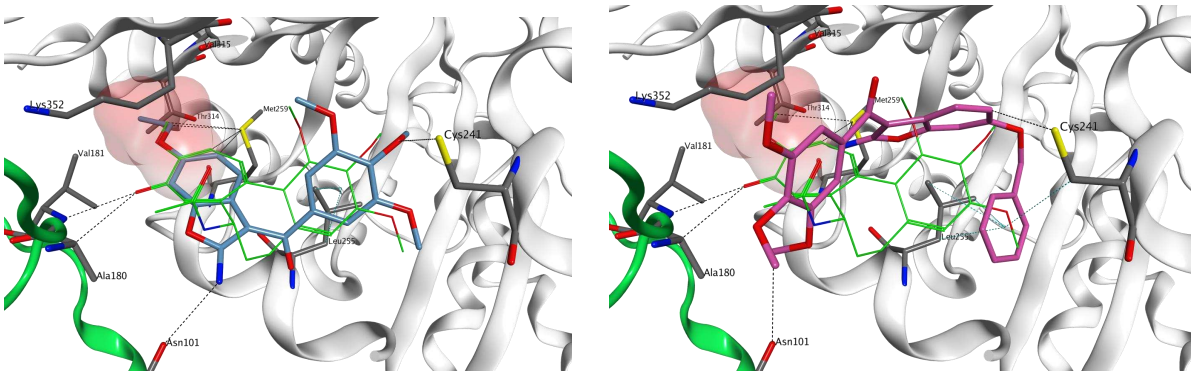

Figure 2. A) Proposed binding mode for compound **4f** in the colchicine site. The trimethoxyphenyl ring is in proximity of βCys241, while the 6-ethoxy substituent lies in the small sub-pocket. B) The benzyl group at the C-6 position cannot be accommodated in the small sub-pocket, and, therefore, compound **4i** is forced away from the binding site. The co-crystallized colchicine is shown in green. The hydrophobic sub-pocket is highlighted with a red surface. The tubulin α-subunit is shown as green ribbon, while the β-subunit is represented in white ribbon. Secondary structure from residue 245 to residue 250 of the β-subunit is not shown for clarity of the structure.

Finally, based on the modeling results, the loss of activity of C-4 methoxy analogue **4b** could be due to the lack of space in the colchicine site around βLeu255, to accommodate the substituent at the C-4 position of the benzo[*b*]furan. Larger substituents than a hydroxyl group at the C-7 position, such as methoxy and ethoxy moieties for derivatives **4e** and **4h**, respectively, could also be sterically hindered by the amino acids αAla180 and αVal181, impeding efficient binding to the colchicine site, thereby reducing antiproliferative activity.

*3.5 Compounds **4f** and **4l** induced alteration of the microtubule network.*

To gain further insight into the tubulin binding effect of test compounds on microtubule structure, morphological characteristics of the microtubules were analyzed by immunofluorescence staining using an anti-β-tubulin antibody in Hela cells after treatment

with compounds **4f** and **4l**. As depicted in Figure 3, microtubule networks in control cells (Ctr) show normal arrangement and intact organization, while after a 24 h treatment, even at the lowest concentration used (10 nM), microtubules show the beginnings of disorganization. At higher concentrations (50 and 100 nM), the effects on microtubules are much more evident, and the cells show clear signs of apoptosis.

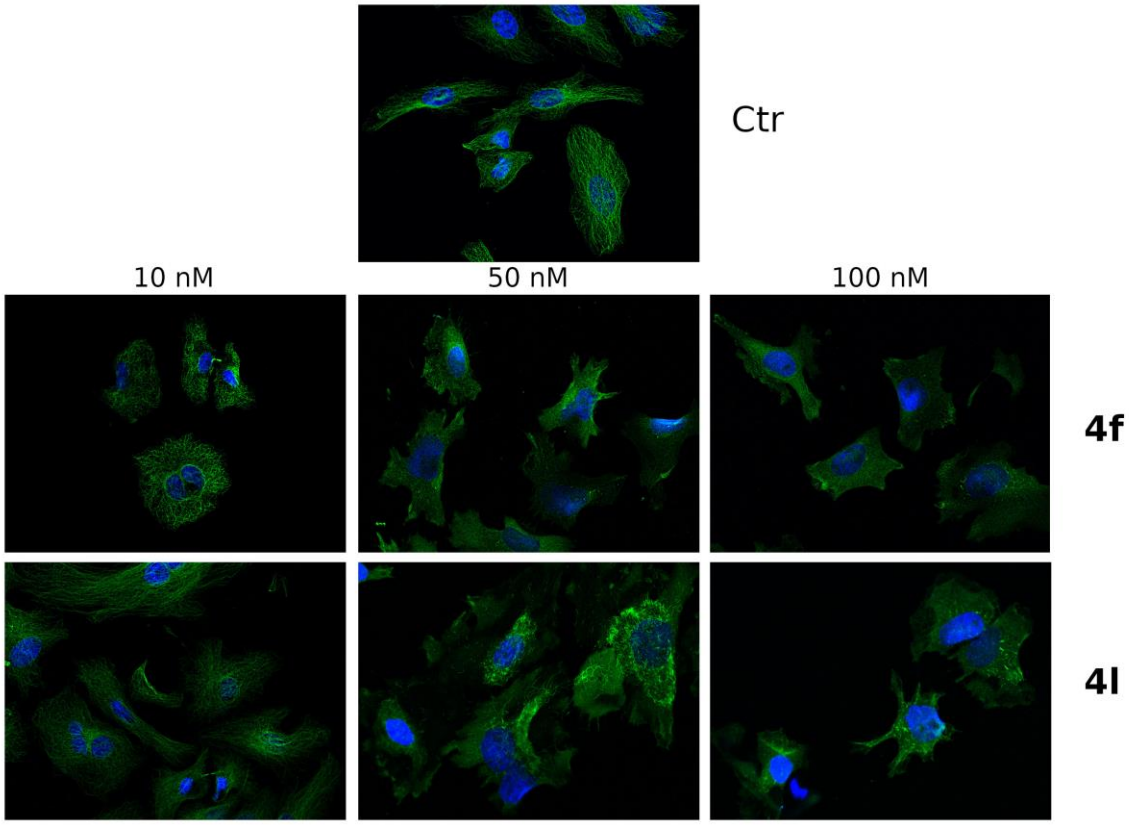

Figure 3. Representative images of microtubule organization in Hela cells treated with **4f** and **4l** at the indicated concentrations for 24 h. HeLa cells were stained with an anti-β-tubulin antibody (green) and DAPI (blue) and then observed by confocal microscopy (Magnification 20X).

*3.6. Compounds **4f** and **4l** induced cell cycle arrest in G2/M and alteration of cell cycle checkpoint proteins.*

The effects of two of the most active compounds (**4f** and **4l**) on cell cycle progression were examined by flow cytometry in HeLa cells (Figure 4). After a 24 h treatment, both compounds induced a G2/M arrest in these cells at a very low concentration (10 nM). With both compounds, the increase in G2/M cells was accompanied by a strong reduction of cells in the G1 phase whereas the S phase was not affected.

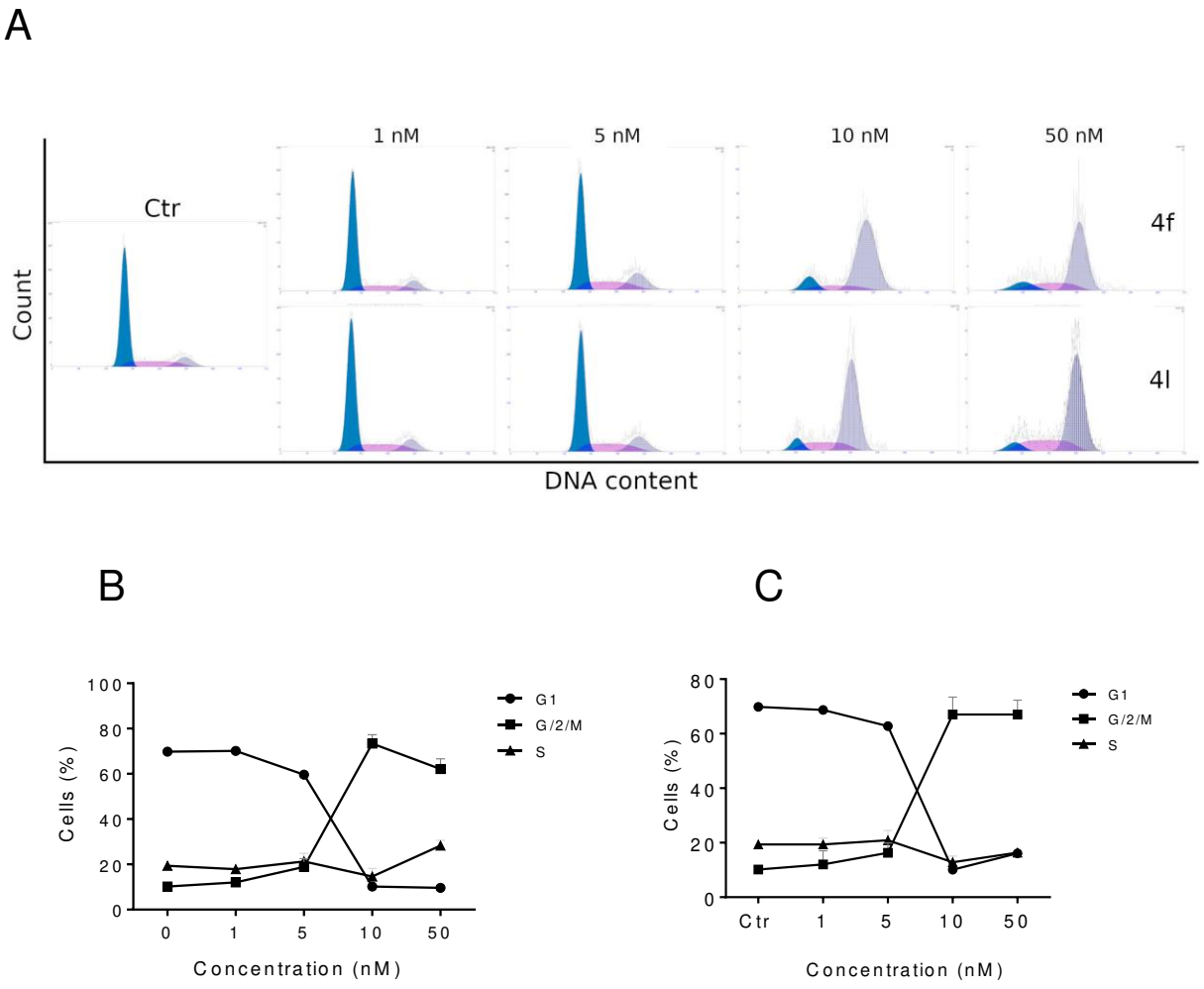

Figure 4. Panel A; representative histograms of cell cycle analysis of HeLa cells treated for 24 h with **4f** or **4l** at the indicated concentrations. Panels B and C: quantitative analysis of the different cell cycle phase in Hela cells. Cells were fixed and labeled with PI and analyzed by flow cytometry as described in the Experimental Section. Data are presented as means of two independent experiments ± SEM.

In addition to analyzing the cell cycle, we wanted to study the effects of **4f** on important checkpoint proteins, such as Bubr1 and Mad-2. These two proteins belong to the spindle assembly checkpoint (SAC), a system that arrests cell cycle progression until microtubule attachment to kinetochores is complete [42]. Cells with depleted or down regulated BubR1 or MAD-2 often undergo apoptotic cell death [43].

As shown in Figure 5, the expression of both BubR1 and MAD-2 was strongly reduced by treatment with **4f** both at 24 and 48 h, and this effect was evident even at the lowest concentration used (10 nM), suggesting mitotic checkpoint abrogation.

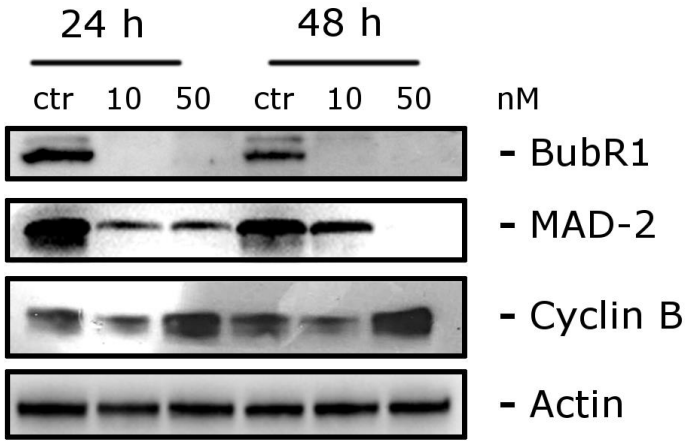

Figure 5. Effect of compound **4f** on cell cycle regulatory proteins. HeLa cells were treated for 24 or 48 h with the indicated concentration of **4f**. The cells were harvested and lysed for the detection of cyclin B, BubR1 and MAD-2 expression by western blot analysis. To confirm equal protein loading, each membrane was stripped and reprobed with anti-β-actin antibody.

Cyclin B1 is a cell cycle regulatory protein involved in mitosis and mainly expressed during the G2/M phase of cell cycle, and it has been demonstrated that cyclin B1 increases after

treatment with antimitotic compounds [44, 45]. Compound **4f**, as shown in Figure 5, induced a dose dependent increase in cyclin B expression, consistent with the rapid accumulation of cells in the G2/M phase.

*3.7. Compounds **4f** and **4l** induced apoptosis through the mitochondrial pathway.*

To characterize the mode of cell death induced by **4f** and **4l**, a biparametric cytofluorimetric analysis was performed using PI, which stains DNA and enters only dead cells, and fluorescent immunolabeling of the protein annexin-V, which binds to phosphatidylserine (PS) in a highly selective manner. Dual staining for annexin-V and with PI permits discrimination between live cells (annexin-V^-/PI^-), early apoptotic cells (annexin-V^+/PI^-), late apoptotic cells (annexin-V^+/PI^+) and necrotic cells (annexin-V^-/PI^+). HeLa cells treated with both compounds at different concentrations showed an increased percentage of annexin-V positive cells (Figure 6, Panels A and B) in a concentration and time-dependent manner. Induction of apoptosis was significant with both compounds even at 10 nM.

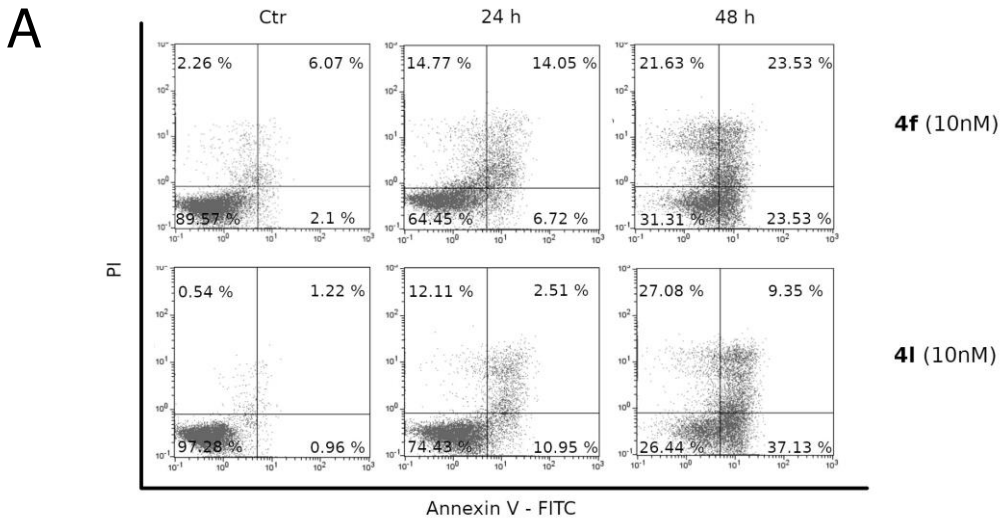

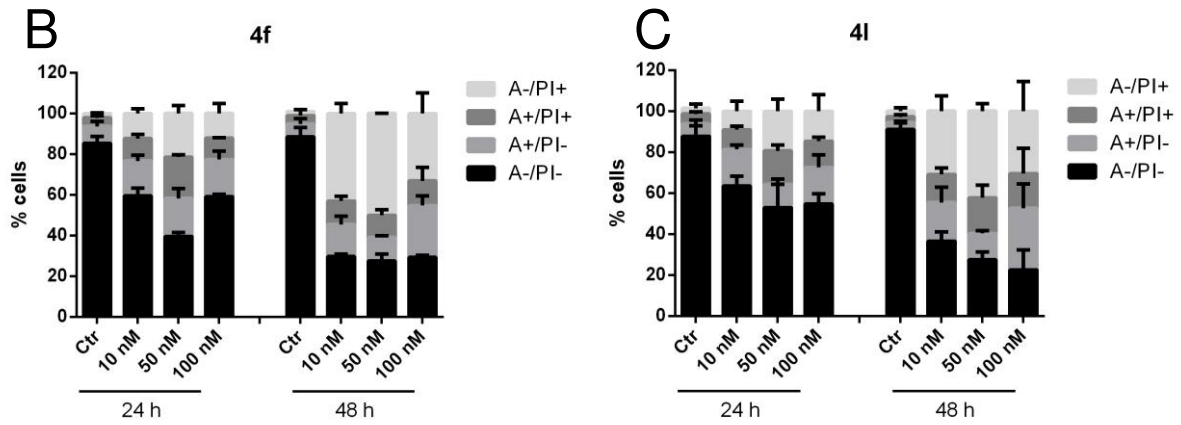

Figure 6. Representative flow cytometric analysis of apoptotic cells after treatment of HeLa cells with compounds **4f** and **4l** at the indicated concentrations after incubation for 24 or 48 h (Panel A). The cells were harvested and labeled with annexin-V-FITC and PI and analyzed by flow cytometry. Panels B and C. Quantitative analysis of apoptotic cells. Data are represented as mean ± SEM of three independent experiments.

Since it has been demonstrated that many anti-mitotic drugs induce apoptosis through the mitochondrial pathway, we also examined whether **4f** and **4l** were able to alter the mitochondrial transmembrane potential ($\Delta\psi_{mt}$) [46-48]. Flow cytometric experiments were performed utilizing the dye 5,5',6,6'-tetrachloro-1,1',3,3'-tetraethylbenzimidazolcarbocyanine (JC-1) [49]. HeLa cells exposed to different concentrations of **4f** and **4l** showed an increased proportion of cells with depolarized mitochondria (Figure 7, Panels B and C).

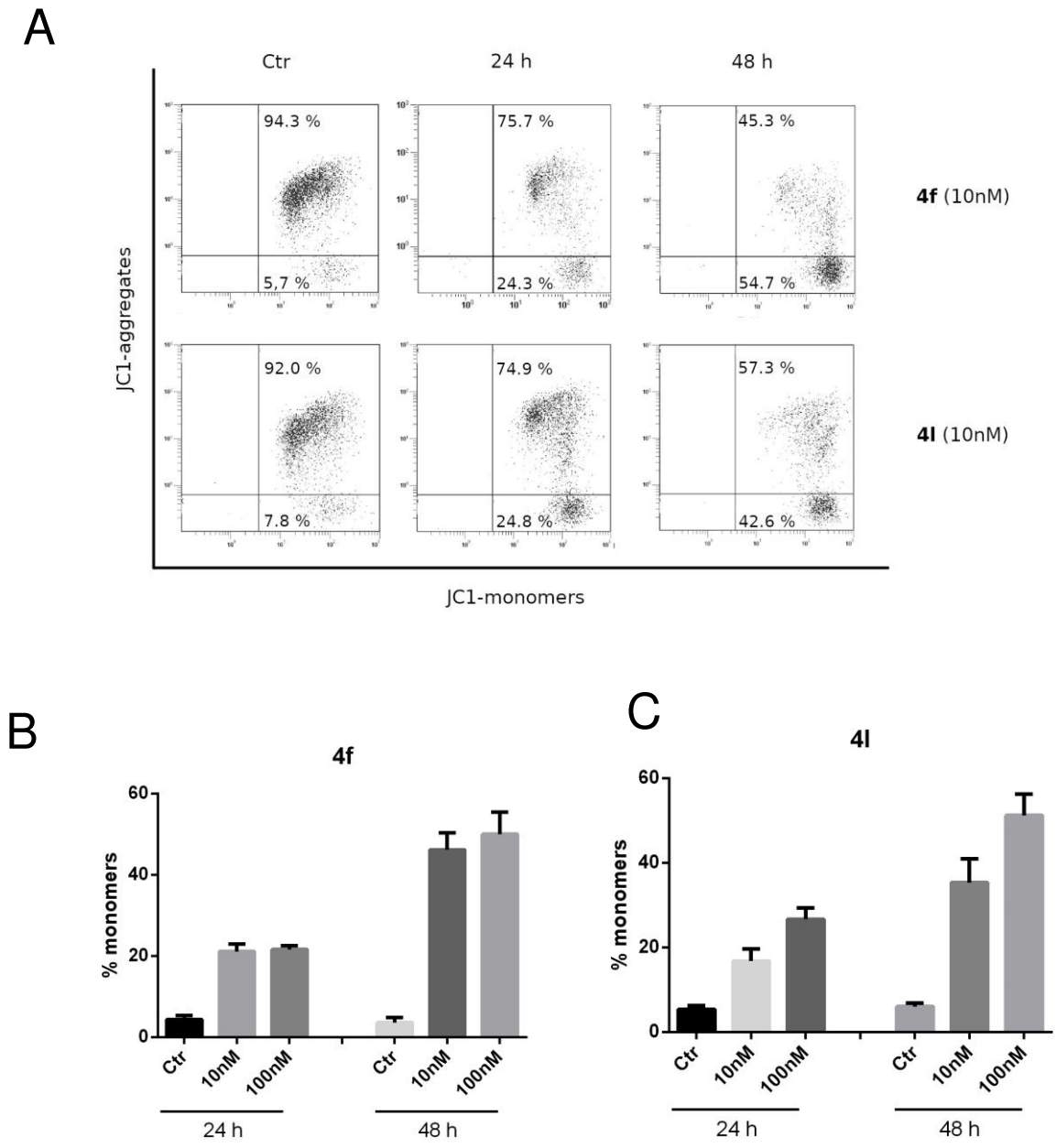

Figure 7. Compounds **4f** and **4l** induce mitochondrial depolarization (Panel A). Hela cells were treated for 24 or 48 h with the indicated concentrations of **4f** (Panel B) or **4l** (Panel D) and then analyzed by flow cytometry using the fluorescent probe JC-1. Data are represented as mean ± SEM of JC-1 monomers demonstrating mitochondrial membrane depolarization from three independent experiments.

*3.8. Compound **4f** induced caspase-9 activation and PARP cleavage.*

Caspase activation is a fundamental process in apoptotic cell death [50]. Caspase-9 is an initiator caspase that is activated early in the apoptotic process by the release of cytochrome-c from the mitochondrion following mitochondrial depolarization [51]. Consequently, the activation of this caspase constitutes a key element of the intrinsic (mitochondrial) apoptotic pathway. As shown in Figure 8, compound **4f** induced cleavage of caspase-9 after a 24 h treatment at the lowest concentration used (10 nM). Moreover, we also observed PARP cleavage, demonstrating at 24 h a fragment of 89 kDa, and this finding is a hallmark of apoptotic cell death [52]. There was a further increase in this fragment after 48 h of treatment at 10 nM **4f**. These results showed that **4f**-induced apoptosis is caspase-dependent, in addition to utilizing the intrinsic (mitochondrial) pathway.

*3.9. Compound **4f** induced Bcl-2 phosphorylation and Mcl-1 downregulation.*

The apoptotic process is regulated by a fine balance between pro-apoptotic and antiapoptotic proteins. Among the latter, Bcl-2 and Mcl-1 are heavily involved in apoptosis induced by antimitotic agents [53]. In this context we found that Bcl-2 is phosphorylated upon treatment with **4f** both at 24 and 48 h (Figure 8). In this context Bcl-2 phosphorylation has been shown to occur with many antimitotic agents, and it is considered a priming event for apoptosis [54]. Furthermore, the expression of Mcl-1 was strongly reduced after a 24 h treatment with **4f** at 10 nM, in agreement with recent studies that underlined the importance of Mcl-1 degradation in response to antimitotic agents and that this event potentiates cell death [55, 56].

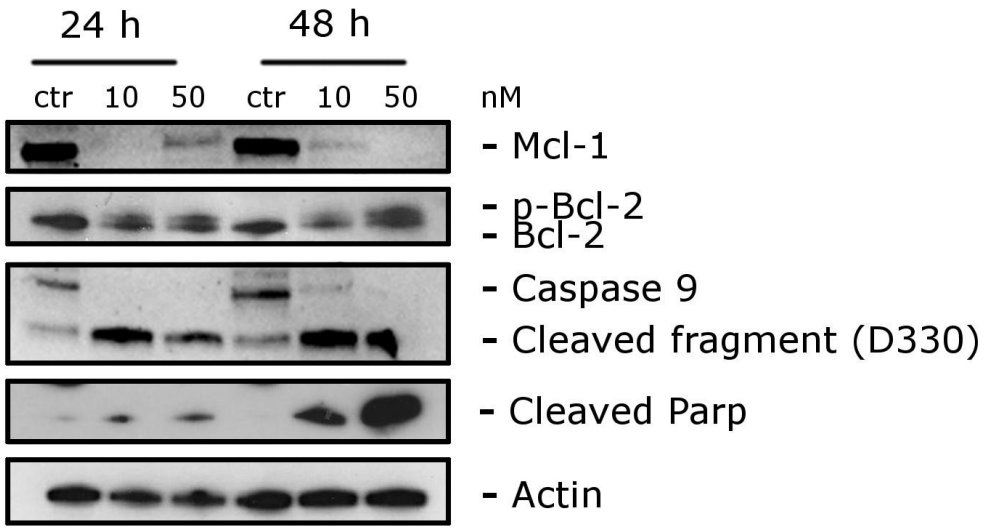

Figure 8. Western blot analysis of caspase-9, PARP, Bcl-2 and Mcl-1 after treatment of HeLa cells with **4f** at the indicated concentrations and for the indicated times. To confirm equal protein loading, each membrane was stripped and reprobed with anti-β-actin antibody.

*3.10. Compound **4f** induces inhibition of capillary-like tubule formation by HUVECs.*

Tubulin binding agents show antivascular effects against tumor endothelium [8, 57-58]. In this context, we evaluated **4f** for its effects on endothelial cells utilizing HUVECs as a model to study angiogenesis in vitro.

To evaluate the antivascular activity of **4f**, we analyzed the ability of the compound to disrupt the "tubule-like" structures formed by HUVECs seeded on Matrigel, a well known *in vitro* angiogenesis test. As shown in Figure 9 (Panel A), after only a 1 h incubation, compound **4f** at 10 nM, as well as at the cytotoxic concentration of 100 nM, clearly disrupted the network of HUVECs as compared with the control. Image analysis [58] was performed to obtain a quantitative assessment of the segment length of the tubules, the area and the number of meshes, the percent of area covered by HUVECs, and the number of branching points after a 1 h treatment (Figure 9, Panels B-G). For segment length and meshes area, a statistically significant effect was observed at 10 nM **4f**, suggesting the high potential of **4f** for vascular disruption.

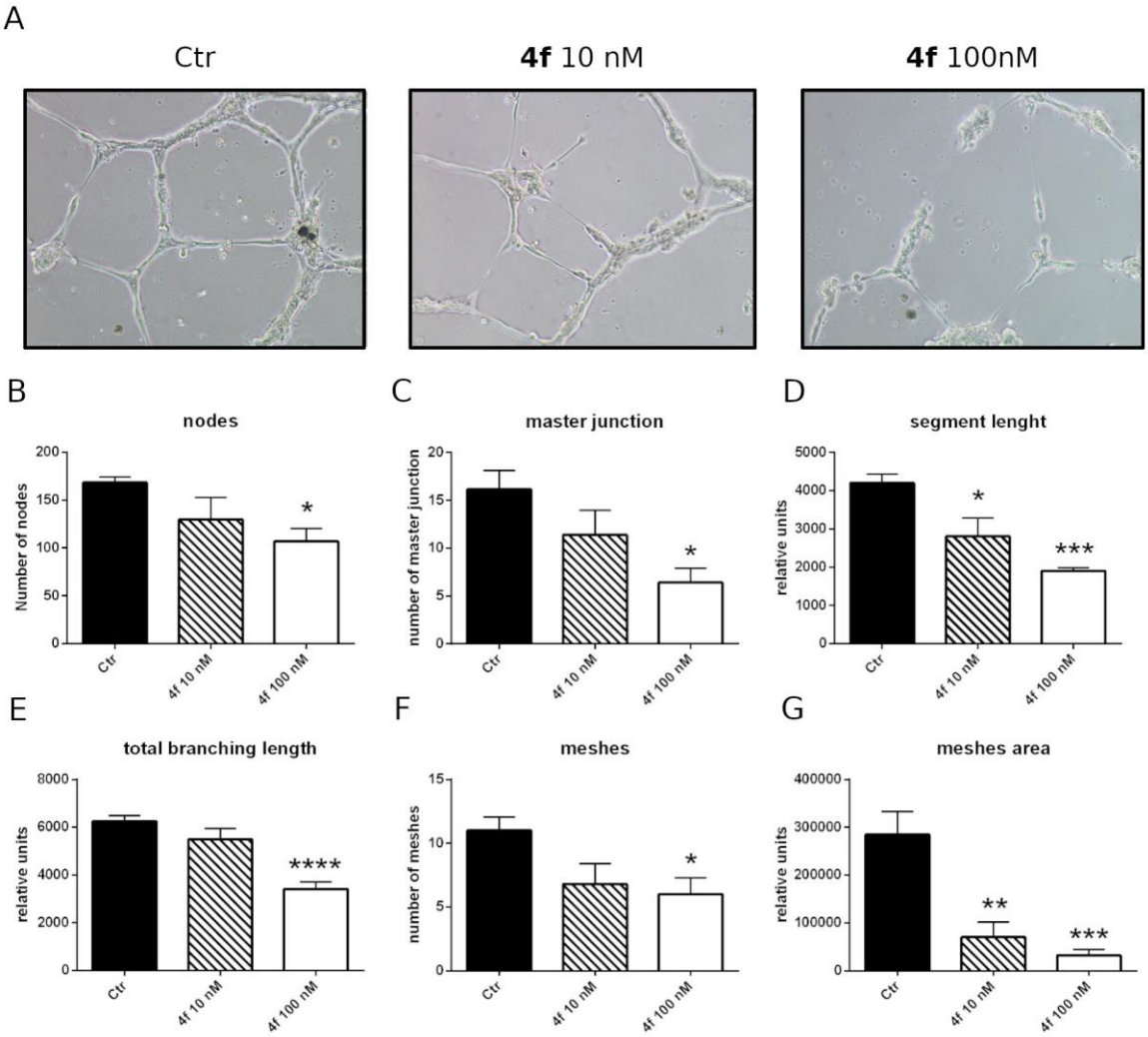

Figure 9. Inhibition of endothelial cell capillary-like tubules formation by **4f**. Tubule formation on Matrigel was examined as described in Materials and Methods. Panel A. Representative images of preformed capillary-like tubules treated with **4f** for 1 h at 10 and 100 nM. Panels B-G. quantitative analysis of the effects of **4f** on the dimensional and topological parameters of the preformed capillary-like tubule network. Data are represented as mean ± SEM of three independent experiments. **p<0.01; ***p<0.001

*3.11. Compound **4f** reduced tumor growth in an orthotopic murine tumor model.*

The antitumor effect *in vivo* of compound **4f** was evaluated in a syngeneic mouse tumor model [59]. This model consists of the use of E0771 murine breast cancer cells orthotopically injected into the mammary fat pad of C57BL/6 female mice. Preliminary experiments were

also carried out to determine the cytotoxicity of **4f** in this cell line. The results of the MTT tests after 72 h of cell treatment indicated a GI_{50} of 15.6 nM, comparable to those observed in the human cancer cell lines.

Compound **4f** was administered by the intraperitoneal route every other day at two different doses (5.0 or 15 mg/kg). As reference compound, CA-4P (**1b**) was used at a dose of 30 mg/kg. As shown in Figure 10A-B, treatment with compound **4f** significantly reduced tumor growth in a dose-dependent manner. When compared with the control group, the tumor mass was reduced by 45.7% and 16.9% with **4f** at 15 and 5 mg/kg, respectively. Treatment with CA-4P reduced tumor growth by 26.5%. These data confirmed the higher potency of **4f** at 15 mg/kg as compared with CA-4P at 30 mg/kg ($p<0.01$). Moreover, even at the higher dose (15 mg/kg), **4f** did not show any sign of toxicity and did not cause a decrease in animal body weight (Figure 10C).

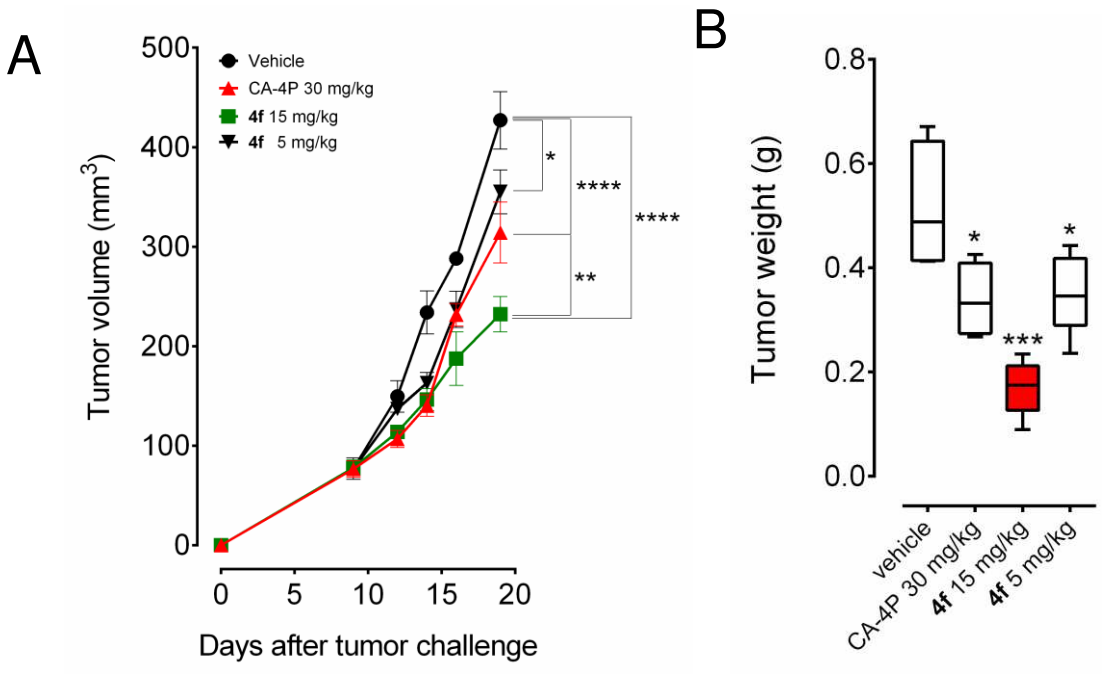

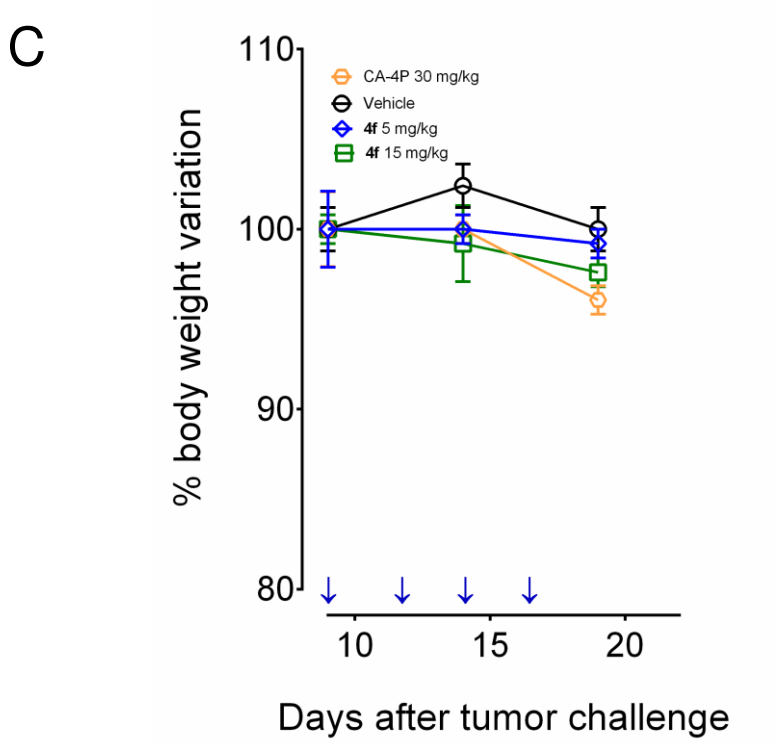

Figure 10. Inhibition of mammary tumor growth in the syngeneic orthotopic E0771-C57BL/6 mouse model by compound **4f**. Female C57BL/6 mice were injected orthotopically in the mammary fat pad with $4x10^5$ E0711 murine breast cancer cells. Tumor-bearing mice were administered the vehicle, as control, or 5.0 or 15 mg/kg of **4f,** or CA-4P as reference compound at 30 mg/kg. Injections were given intraperitoneally on the days indicated by the arrows. Data are presented as mean ± SEM of tumor volume at each time point (Panel A) or tumor weight (Panel B) measured at the end of the experimental procedure (*n*= 5 mice/group). Panel C represents the animal body weight variation during the treatment period. Asterisks indicate a significant difference between the treated and the control group. * $p < 0.05$, ** $p < 0.01$, **** $p < 0.0001$.

4. Conclusions

We have reported the synthesis and biological evaluation of a new class of synthetic antitubulin compounds based on the 2-amino-3-(3',4',5'-trimethoxybenzoyl)benzo[*b*]furan molecular skeleton. Structure-activity relationships were investigated by the insertion of electron-withdrawing or electron releasing substituents at one of positions C-4 to C-7 of the

benzo[*b*]furan scaffold. The C-6 ethoxy derivative **4f** and the C-6 methyl analogue **4l** were the two most potent compounds of the series, exhibiting IC_{50} values of 0.005-2.8 and 0.3-3.5 nM, respectively, as compared with the range 0.8-3100 nM obtained with CA-4 in cancer cell lines. A major finding with **4f** was its highly potent activity (IC_{50}: 5 pM) against Daoy cells. Although **4f** was 3-fold less potent than CA-4 against HL-60 cells, it was from 1.5- to 2,460-fold more active than CA-4 against the other five cancer cell lines. While compounds **4f** and **4l** had potent antiproliferative activity against the Daoy medulloblastoma cell line, both derivatives had IC_{50} values greater than 10 μM against normal human astrocytes, suggesting low toxicity in normal cells in comparison to tumor cells.

Selected molecules (**3c**, **4c-d**, **4f-g**. and **4k-l**) showed potent inhibition of tubulin assembly and the binding of colchicine to tubulin, and **4f** and **4l** were better inhibitors of assembly than CA-4. For the most active compounds (C-6 methoxy analogue **4d** along with **4f** and **4l**), a good correlation was observed between antiproliferative activities and inhibition of tubulin assembly and colchicine binding. Thus, the antiproliferative activity of these compounds derived from an interaction with the colchicine site of tubulin and interference with microtubule assembly. This indicated that the cellular actions of these agents would involve mitotic arrest, due to interference with the functions of the mitotic spindle, and their use would ultimately lead to apoptotic cell death. Compound **4f** was also shown to have potential antivascular activity, since it disrupted the network of HUVECs at a concentration of 10 nM. The excellent antitumor efficacy of the most active compound **4f** was demonstrated in an orthotopic murine model of breast cancer, in which we observed significant inhibition of tumor growth occurring at a low dose in comparison to the reference compound CA-4P, and there were no apparent signs of toxicity in the treated mice.

5. Experimental Protocols.

5.1. Chemistry.

5.1.1. Materials and Methods.

^{1}H NMR and ^{13}C NMR spectra were recorded in $CDCl_3$ solution with a Varian Mercury Plus 400 spectrometer at 400 MHz and 100 MHz, respectively. Peak positions are given in parts per million (*ppm*) downfield from tetramethylsilane as internal standard, and *J* values are given in hertz. Positive-ion electrospray ionization (ESI) mass spectra were measured on a double-focusing Finnigan MAT 95 instrument with BE geometry. Analytical HPLC analyses were performed at ambient temperature on a Beckman 125 liquid chromatograph fitted with a Luna C-18 column (4.6 x 100 mm, 3 μm particle size) with 0.1% TFA in H_2O (A) and 0.1% TFA in CH_3CN (B) solvent mixtures and equipped with a Beckman 168 diode array detector. Melting points (mp) were determined on a Buchi-Tottoli apparatus and are uncorrected. All tested compounds yielded data consistent with a purity of at least 95% as compared with the theoretical values. All reactions were carried out under an inert atmosphere of dry nitrogen, unless otherwise indicated. TLC was performed on silica gel (precoated F_{254} Merck plates), and compounds were visualized with aqueous $KMnO_4$. Flash column chromatography was performed using 230-400 mesh silica gel and the indicated solvent system. Organic solutions were dried over anhydrous Na_2SO_4. All commercial chemicals and solvents were reagent grade and were used without further treatment. With the exception of compounds **5f-g** and **5n**, all salicyladehydes are commercially available.

*5.1.2. General procedure for the synthesis of compounds **6a-n**.*

A mixture of the appropriate salicylaldehyde **5a-n** (1 mmol), 2-azido-1-(3,4,5-trimethoxyphenyl)ethanone (0.25 g, 1 mmol) and piperidinium acetate (0.15 g, 1 mmol) in

methanol (5 mL) was stirred in the dark for 24 h at room temperature. If the α-azidochalcone precipitated from the reaction mixture, the solid was collected by filtration, washed with cold methanol, dried under vacuum and used without further purification for the next reaction. When the α-azidochalcone did not precipitate, the reaction mixture was evaporated to dryness under reduced pressure, and the resulting residue suspended in a mixture of 50% ethyl acetate and 50% water. After phase separation, the organic layer was washed with brine, dried over Na_2SO_4 and concentrated under vacuum to give a crude product, which was purified by silica-gel column chromatography to yield the appropriate α-azidochalcone.

*5.1.2.1. (Z)-2-Azido-3-(2-hydroxyphenyl)-1-(3,4,5-trimethoxyphenyl)prop-2-en-1-one (**6a**).* The crude residue purified by flash chromatography, using EtOAc:petroleum ether 1:1 (v:v) for elution, furnished **6a** as a yellow oil. Yield 64%. ^{1}H-NMR (DMSO-d_6) δ: 3.78 (s, 3H), 3.84 (s, 6H), 6.84 (m, 2H), 7.02 (s, 1H), 7.14 (s, 2H), 7.22 (m, 1H), 8.18 (dd, J=7.2 and 2.4 Hz, 1H), 10.1 (s, 1H).

*5.1.2.2. (Z)-2-Azido-3-(2-hydroxy-6-methoxyphenyl)-1-(3,4,5-trimethoxyphenyl)prop-2-en-1-one (**6b**).* The precipitate was collected by filtration and washed with cold methanol, to furnish **6b** as a cream-colored solid. Yield 63%, mp 130-132 °C. ^{1}H-NMR (DMSO-d_6) δ: 3.77 (s, 6H), 3.86 (s, 6H), 6.49 (d, J=8.2 Hz, 1H), 6.65 (s, 1H), 7.19 (m, 4H), 9.82 (bs, 1H).

*5.1.2.3. (Z)-2-Azido-3-(2-hydroxy-5-methoxyphenyl)-1-(3,4,5-trimethoxyphenyl)prop-2-en-1-one (**6c**).* The precipitate was collected by filtration and washed with cold methanol, to furnish **6c** as a yellow solid. Yield 69%, mp 97-99 °C. ^{1}H-NMR (DMSO-d_6) δ: 3.72 (s, 3H), 3.78 (s, 3H), 3.84 (s, 6H), 6.82 (m, 2H), 7.00 (s, 1H), 7.12 (s, 2H), 7.74 (d, J=2.6 Hz, 1H), 9.70 (s, 1H).

*5.1.2.4. (Z)-2-Azido-3-(2-hydroxy-4-methoxyphenyl)-1-(3,4,5-trimethoxyphenyl)prop-2-en-1-one (**6d**).* The crude residue purified by flash chromatography, using EtOAc:petroleum ether 4:6 (v:v) for elution, furnished **6d** as a yellow solid. Yield 86%, mp 112-114 °C. ^{1}H-NMR (DMSO-d_6) δ: 3.74 (s, 3H), 3.77 (s, 3H), 3.83 (s, 6H), 6.42 (d, J=2.2 Hz, 1H), 6.46 (dd, J=9.0 and 2.2 Hz, 1H), 7.05 (s, 1H), 7.08 (s, 2H), 8.18 (d, J=9.0 Hz, 1H), 10.3 (s, 1H).

*5.1.2.5. (Z)-2-Azido-3-(2-hydroxy-3-methoxyphenyl)-1-(3,4,5-trimethoxyphenyl)prop-2-en-1-one (**6e**).* The precipitate was collected by filtration and washed with cold methanol, to furnish **6e** as a white solid. Yield 75%, mp 130-131 °C. ^{1}H-NMR (DMSO-d_6) δ: 3.78 (s, 3H), 3.80 (s, 3H), 3.83 (s, 6H), 6.85 (t, J=8.0 Hz, 1H), 6.98 (dd, J=8.0 and 1.2 Hz, 1H), 7.07 (s, 1H), 7.12 (s, 2H), 7.77 (dd, J=8.0 and 1.2 Hz, 1H), 9.42 (bs, 1H).

*5.1.2.6. (Z)-2-Azido-3-(2-hydroxy-4-ethoxyphenyl)-1-(3,4,5-trimethoxyphenyl)prop-2-en-1-one (**6f**).* The crude residue purified by flash chromatography, using EtOAc:petroleum ether 4:6 (v:v) for elution, furnished **6f** as a yellow solid. Yield 68%, mp 135-137 °C. ^{1}H-NMR (DMSO-d_6) δ: 1.31 (t, J=6.8 Hz, 3H), 3.77 (s, 3H), 3.83 (s, 6H), 4.02 (q, J=6.8 Hz, 2H), 6.41 (d, J=2.2 Hz, 1H), 6.47 (dd, J=8.8 and 2.2 Hz, 1H), 7.05 (s, 1H), 7.07 (s, 2H), 8.17 (d, J=8.8 Hz, 1H), 10.3 (s, 1H).

*5.1.2.7. (Z)-2-Azido-3-(2-hydroxy-4-propoxyphenyl)-1-(3,4,5-trimethoxyphenyl)prop-2-en-1-one (**6g**).* The crude residue purified by flash chromatography, using EtOAc:petroleum ether 3:7 (v:v) for elution, furnished **6g** as a yellow solid. Yield 58%, mp 168-170 °C. ^{1}H-NMR (DMSO-d_6) δ: 0.97 (t, J=7.4 Hz, 3H), 1.74 (m, 2H), 3.76 (s, 3H), 3.83 (s, 6H), 3.91 (q, J=7.4 Hz, 2H), 6.41 (d, J=2.2 Hz, 1H), 6.50 (dd, J=9.0 and 2.2 Hz, 1H), 7.05 (s, 1H), 7.07 (s, 2H), 8.17 (d, J=9.0 Hz, 1H), 10.2 (s, 1H).

*5.1.2.8. (Z)-2-Azido-3-(2-hydroxy-3-ethoxyphenyl)-1-(3,4,5-trimethoxyphenyl)prop-2-en-1-one (**6h**).* The precipitate was collected by filtration and washed with cold methanol, to furnish **6h** as a yellow solid. Yield 67%, mp 138-139 °C. ^{1}H-NMR (DMSO-d_6) δ: 1.33 (t, J=7.0 Hz, 3H), 3.77 (s, 3H), 3.84 (s, 6H), 4.03 (q, J=7.0 Hz, 2H), 6.83 (t, J=8.0 Hz, 1H), 6.97 (d, J=8.0 Hz, 1H), 7.08 (s, 1H), 7.13 (s, 2H), 7.76 (d, J=8.0 Hz, 1H), 9.12 (s, 1H).

*5.1.2.9. (Z)-2-Azido-3-(2-hydroxy-4-benzyloxyphenyl)-1-(3,4,5-trimethoxyphenyl)prop-2-en-1-one (**6i**).* The crude residue purified by flash chromatography, using EtOAc:petroleum ether 1:1 (v:v) for elution, furnished **6i** as a yellow solid. Yield 71%, mp 102-104 °C. ^{1}H-NMR (DMSO-d_6) δ: 3.77 (s, 3H), 3.82 (s, 6H), 5.10 (s, 2H), 6.48 (d, J=2.4 Hz, 1H), 6.58 (dd, J=8.8 and 2.4 Hz, 1H), 7.04 (s, 1H), 7.07 (s, 2H), 7.42 (m, 5H), 8.18 (d, J=9.0 Hz, 1H), 10.3 (s, 1H).

*5.1.2.10. (Z)-2-Azido-3-(2-hydroxy-4-fluorophenyl)-1-(3,4,5-trimethoxyphenyl)prop-2-en-1-one (**6j**).* The crude residue purified by flash chromatography, using EtOAc:petroleum ether 3:7 (v:v) for elution, furnished **6j** as a yellow solid. Yield 55%, mp 107-109 °C. ^{1}H-NMR (DMSO-d_6) δ: 3.77 (s, 3H), 3.83 (s, 6H), 6.68 (m, 2H), 6.96 (s, 1H), 7.11 (s, 2H), 8.12 (dd, J=8.4 and 5.6 Hz, 1H), 10.8 (bs, 1H).

*5.1.2.11. (Z)-2-Azido-3-(2-hydroxy-4-bromophenyl)-1-(3,4,5-trimethoxyphenyl)prop-2-en-1-one (**6k**).* The precipitate was collected by filtration and washed with cold methanol, to furnish **6k** as a white solid. Yield 60%, mp 115-117 °C. ^{1}H-NMR (DMSO-d_6) δ: 3.77 (s, 3H), 3.83 (s, 6H), 6.93 (s, 1H), 7.02 (m, 2H), 7.12 (s, 2H), 8.09 (d, J=8.2 Hz, 1H), 10.2 (bs, 1H).

*5.1.2.12. (Z)-2-Azido-3-(2-hydroxy-4-methylphenyl)-1-(3,4,5-trimethoxyphenyl)prop-2-en-1-one (**6l**).* The precipitate was collected by filtration and washed with cold methanol, to furnish **6l** as a yellow solid. Yield 56%, mp 100-102 °C. ^{1}H-NMR (DMSO-d_6) δ: 2.24 (s, 3H), 3.77

(s, 3H), 3.83 (s, 6H), 6.68 (m, 2H), 7.05 (s, 1H), 7.09 (s, 2H), 8.08 (d, J=7.8 Hz, 1H), 10.2 (s, 1H).

*5.1.2.13. (Z)-2-Azido-3-(2-hydroxy-5-nitrophenyl)-1-(3,4,5-trimethoxyphenyl)prop-2-en-1-one (**6m**).* The precipitate was collected by filtration and washed with cold methanol, to furnish **6m** as a yellow solid. Yield 53%, mp 137-138 °C. ^{1}H-NMR (DMSO-d_6) δ: 3.78 (s, 3H), 3.84 (s, 6H), 6.85 (s, 1H), 7.01 (d, J=7.8 Hz, 1H), 7.17 (s, 2H), 8.12 (d, J=7.8 Hz, 1H), 9.02 (s, 1H), 11.8 (s, 1H).

*5.1.2.14. (Z)-2-Azido-3-(2,3-dihydroxy-4-methoxyphenyl)-1-(3,4,5-trimethoxyphenyl)prop-2-en-1-one (**6n**).* The crude residue purified by flash chromatography, using EtOAc:petroleum ether 1:1 (v:v) for elution, furnished **6n** as a yellow solid. Yield 36%, mp 121-123 °C. ^{1}H-NMR (DMSO-d_6) δ: 3.77 (s, 3H), 3.83 (s, 6H), 3.87 (s, 3H), 6.58 (d, J=9.0 Hz, 1H), 7.08 (s, 2H), 7.09 (s, 1H), 7.75 (d, J=9.0 Hz, 1H), 9.13 (s, 1H), 10.3 (s, 1H).

*5.1.3. General procedure for the synthesis of compounds **3c**, **4a-l** and **7a**.*

A mixture of the appropriate α-azidochalcone **6a-n** (1 mmol) and *p*-TSA (38 mg, 0.2 mmol) in acetonitrile (10 mL) was stirred under argon at reflux for 12 h (Method A) or irradiated with a 25W white CFL for 24 h at room temperature (Method B). After this time, the reaction mixture was concentrated under reduced pressure to give a residue that was dissolved in dichloromethane (15 mL) and washed with water (5 mL) and brine (5 mL). The organic layer was dried on Na_2SO_4, filtered and evaporated. The crude product was purified by silica gel column chromatography to yield compounds **3c, 4a-l** and **7a.**

*5.1.3.1. (2-Amino-7-hydroxy-6-methoxybenzofuran-3-yl)(3,4,5-trimethoxyphenyl)methanone (**3c**).* The crude residue purified by flash chromatography, using EtOAc:petroleum ether 6:4 (v:v) for elution, furnished **3c** as a yellow solid. Yield: 71% (Method A), 52% (Method B),

mp 103-105 °C. ^{1}H-NMR (DMSO-d_6) δ: 3.73 (s, 3H), 3.75 (s, 6H), 3.77 (s, 3H), 6.21 (d, J=8.8 Hz, 1H), 6.69 (d, J=8.8 Hz, 1H), 6.89 (s, 2H), 8.47 (bs, 2H), 9.25 (s, 1H). ^{13}C-NMR (DMSO-d_6) δ: 55.83 (2C), 56.75, 60.08, 91.92, 104.46 (2C), 107.41, 108.82, 121.28, 122.49, 131.49, 136.49, 139.02, 143.81, 152.51 (2C), 166.90, 187.32. MS (ESI): $[M+1]^+$=374.22. HPLC: t_R=15.97 min.

*5.1.3.2. (2-Amino-benzofuran-3-yl)(3,4,5-trimethoxyphenyl)methanone (**4a**).* The crude residue purified by flash chromatography, using EtOAc:petroleum ether 1:1 (v:v) for elution, furnished **4a** as a yellow solid. Yield: 73% (Method A), 49% (Method B), mp 103-104 °C. ^{1}H-NMR (DMSO-d_6) δ: 3.74 (s, 3H), 3.75 (s, 6H), 6.82 (dd, J=6.8 and 1.6 Hz, 1H), 6.89 (s, 2H), 6.99 (m, 2H), 7.30 (dd, J=7.6 and 2.0 Hz, 1H), 8.54 (s, 2H). ^{13}C-NMR (DMSO-d_6) δ: 56.39 (2C), 60.66, 92.43, 105.08 (2C), 110.36, 118.55, 121.78, 123.96, 126.89, 136.85, 139.79, 148.85, 153.15 (2C), 167.25, 188.14. MS (ESI): $[M+1]^+$=328.43. HPLC: t_R=20.20 min.

*5.1.3.3. (2-Amino-4-methoxybenzofuran-3-yl)(3,4,5-trimethoxyphenyl)methanone (**4b**).* The crude residue purified by flash chromatography, using EtOAc:petroleum ether 1:1 (v:v) for elution, furnished **4b** as a yellow solid. Yield: 74% (Method A), 53% (Method B), mp 123-125 °C. ^{1}H-NMR (DMSO-d_6) δ: 3.28 (s, 3H), 3.69 (s, 6H), 3.72 (s, 3H), 6.69 (dd, J=6.8 and 2.4 Hz, Hz, 1H), 6.81 (s, 2H), 7.05 (m, 2H), 8.22 (bs, 2H). ^{13}C-NMR (DMSO-d_6) δ: 54.79, 55.67 (2C), 59.99, 91.72, 102.97, 105.52 (2C), 106.22, 115.17, 122.17, 137.32, 139.31, 149.04, 151.21, 151.62 (2C), 165.71, 188.15. MS (ESI): $[M+1]^+$=358.31. HPLC: t_R=16.83 min.

*5.1.3.4. (2-Amino-5-methoxybenzofuran-3-yl)(3,4,5-trimethoxyphenyl)methanone (**4c**).* The crude residue purified by flash chromatography, using EtOAc:petroleum ether 1:1 (v:v) for

elution, furnished **4c** as a cream-colored solid. Yield: 68% (Method A), 49% (Method B), mp 140-142 °C. ^{1}H-NMR (DMSO-*d*$_6$) δ: 3.56 (s, 3H), 3.74 (s, 3H), 3.78 (s, 6H), 6.26 (d, J=2.4 Hz, 1H), 6.56 (dd, J=8.8 and 2.4 Hz, 1H), 6.89 (s, 2H), 7.22 (d, J=8.8 Hz, 1H), 8.54 (bs, 2H). ^{13}C-NMR (DMSO-*d*$_6$) δ: 55.07, 55.88 (2C), 60.09, 92.30, 103.22, 104.36 (2C), 106.91, 109.98, 127.34, 136.36, 139.09, 142.99, 152.64 (2C), 155.78, 167.23, 187.61. MS (ESI): $[M+1]^+$=358.40. HPLC: t_R=17.93 min.

*5.1.3.5. (2-Amino-6-methoxybenzofuran-3-yl)(3,4,5-trimethoxyphenyl)methanone (**4d**).* The crude residue purified by flash chromatography, using EtOAc:petroleum ether 1:1 (v:v) for elution, furnished **4d** as an orange solid. Yield: 74% (Method A), 52% (Method B), mp 48-50 °C. ^{1}H-NMR (DMSO-*d*$_6$) δ: 3.72 (s, 3H), 3.75 (s, 3H), 3.77 (s, 6H), 6.67 (dd, J=9.0 and 2.4 Hz, 1H), 6.73 (d, J=9.0 Hz, 1H), 6.90 (s, 2H), 7.03 (d, J=2.4 Hz, 1H), 8.48 (bs, 2H). ^{13}C-NMR (DMSO-*d*$_6$) δ: 55.51, 55.88 (2C), 60.13, 91.58, 96.60, 104.54 (2C), 110.19, 118.18, 119.22, 136.42, 139.21, 149.12, 152.60 (2C), 155.25, 166,712, 187.11. MS (ESI): $[M+1]^+$=358.28. HPLC: t_R=16.95 min.

*5.1.3.6. (2-Amino-7-methoxybenzofuran-3-yl)(3,4,5-trimethoxyphenyl)methanone (**4e**).* The crude residue purified by flash chromatography, using EtOAc:petroleum ether 6:4 (v:v) for elution, furnished **4e** as a white solid. Yield: 72% (Method A), 48% (Method B), mp 164-165 °C. ^{1}H-NMR (DMSO-*d*$_6$) δ: 3.75 (s, 3H), 3.76 (s, 6H), 3.88 (s, 3H), 6.43 (d, J=7.6 Hz, 1H), 6.71 (d, J=8.0 Hz, 1H), 6.90 (s, 2H), 6.94 (d, J=8.0 Hz, 1H), 8.51 (bs, 2H). ^{13}C-NMR (DMSO-*d*$_6$) δ: 55.68, 55.82 (2C), 60.10, 92.29, 104.64 (2C), 105.11, 110.79, 124.03, 127.87, 136.16, 136.77, 139.25, 143.73, 152.53 (2C), 166.54, 187.68. MS (ESI): $[M+1]^+$=358.39. HPLC: t_R=17.60 min.

*5.1.3.7. (2-Amino-6-ethoxybenzofuran-3-yl)(3,4,5-trimethoxyphenyl)methanone (**4f**).* The crude residue purified by flash chromatography, using EtOAc:petroleum ether 1:1 (v:v) for elution, furnished **4f** as an orange solid. Yield: 78% (Method A), 46% (Method B), mp 83-85 °C. ^{1}H-NMR (DMSO-d_6) δ: 1.29 (t, J=6.8 Hz, 3H), 3.75 (s, 3H), 3.77 (s, 6H), 3.97 (q, J=6.8 Hz, 2H), 6.63 (dd, J=9.0 and 2.4 Hz, 1H), 6.73 (d, J=9.0 Hz, 1H), 6.90 (s, 2H), 7.00 (d, J=2.4 Hz, 1H), 8.46 (bs, 2H). ^{13}C-NMR (DMSO-d_6) δ: 14.55, 55.81 (2C), 60.09, 63.41, 91.56, 97.05, 104.48 (2C), 110.68, 118.15, 119.08, 136.40, 139.14, 149.06, 152.56 (2C), 154.39, 166.65, 187.06. MS (ESI): $[M+1]^+$=372.31. HPLC: t_R=18.62 min.

*5.1.3.8. (2-Amino-6-propoxybenzofuran-3-yl)(3,4,5-trimethoxyphenyl)methanone (**4g**).* The crude residue purified by flash chromatography, using EtOAc:petroleum ether 4:6 (v:v) for elution, furnished **4g** as an orange solid. Yield: 78% (Method A), 52% (Method B), mp 168-170 °C. ^{1}H-NMR (DMSO-d_6) δ: 0.96 (t, J=7.2 Hz, 3H), 1.68 (m, 2H), 3.75 (s, 3H), 3.77 (s, 6H), 3.88 (q, J=7.6 Hz, 2H), 6.64 (dd, J=8.8 and 2.0 Hz, 1H), 6.73 (d, J=8.8 Hz, 1H), 6.90 (s, 2H), 7.01 (d, J=2.0 Hz, 1H), 8.48 (bs, 2H). ^{13}C-NMR (DMSO-d_6) δ: 10.33, 21.95, 55.81 (2C), 60.09, 69.36, 91.55, 97.09, 104.49 (2C), 110.68, 118.16, 119.06, 136.38, 139.14, 149.07, 152.55 (2C), 154.55, 166.69, 187.04. MS (ESI): $[M+1]^+$=386.19. HPLC: t_R=19.85 min.

*5.1.3.9. (2-Amino-7-ethoxybenzofuran-3-yl)(3,4,5-trimethoxyphenyl)methanone (**4h**).* The crude residue purified by flash chromatography, using EtOAc:petroleum ether 1:1 (v:v) for elution, furnished **4h** as an orange solid. Yield: 68% (Method A), 43% (Method B), mp 158-160 °C. ^{1}H-NMR (DMSO-d_6) δ: 1.37 (t, J=6.8 Hz, 3H), 3.75 (s, 3H), 3.76 (s, 6H), 4.14 (q, J=6.8 Hz, 2H), 6.41 (d, J=8.0 Hz, 1H), 6.69 (d, J=8.0 Hz, 1H), 6.90 (s, 2H), 6.94 (t, J=8.0 Hz, 1H), 8.52 (bs, 2H). ^{13}C-NMR (DMSO-d_6) δ: 14.69, 55.83 (2C), 60.12, 63.80, 92.31, 104.60 (2C), 105.78, 110.68, 124.06, 127.92, 136.21, 136.57, 139.19, 142.99, 152.53 (2C), 166.58, 187.68. MS (ESI): $[M+1]^+$=372.39. HPLC: t_R=19.75 min.

*5.1.3.10. (2-Amino-6-benzyloxybenzofuran-3-yl)(3,4,5-trimethoxyphenyl)methanone (**4i**).* The crude residue purified by flash chromatography, using EtOAc:petroleum ether 1:1 (v:v) for elution, furnished **4i** as an orange solid. Yield: 75% (Method A), 54% (Method B), mp 123-125 °C. ^{1}H-NMR (DMSO-*d*$_6$) δ: 3.72 (s, 3H), 3.75 (s, 3H), 3.77 (s, 6H), 6.67 (dd, J=9.0 and 2.4 Hz, 1H), 6.73 (d, J=9.0 Hz, 1H), 6.90 (s, 2H), 7.03 (d, J=2.4 Hz, 1H), 8.48 (bs, 2H). ^{13}C-NMR (DMSO-*d*$_6$) δ: 55.82 (2C), 60.09, 69.69, 91.53, 97.57, 104.49 (2C), 111.07, 118.13, 119.44, 127.71 (2C), 128.28 (2C), 136.37, 136.95, 139.16, 148.96, 152.56 (2C), 154.16, 166.71, 187.07. MS (ESI): $[M+1]^+$=434.37. HPLC: t_R=21.25 min.

*5.1.3.11. (2-Amino-6-fluorobenzofuran-3-yl)(3,4,5-trimethoxyphenyl)methanone (**4j**).* The crude residue purified by flash chromatography, using EtOAc:petroleum ether 1:1 (v:v) for elution, furnished **4j** as a white solid. Yield: 76% (Method A), 44% (Method B), mp 178-180 °C. ^{1}H-NMR (DMSO-*d*$_6$) δ: 3.76 (s, 3H), 3.77 (s, 6H), 6.76 (d, J=8.4 Hz, 1H), 7.21 (dd, J=8.4 and 5.2 Hz, 1H), 6.91 (s, 2H), 7.35 (dd, J=9.2 and 2.8 Hz, 1H), 8.56 (bs, 2H). ^{13}C-NMR ($CDCl_3$) δ: 56.31 (2C), 61.12, 93.76, 98.791 and 99.057 ($^{2}J_{CF}$=26.6 Hz), 105.00 (2C), 110.936 and 111.165 ($^{2}J_{CF}$=22.9 Hz), 110.94, 119.330 and 119.421 ($^{3}J_{C-F}$=9.1 Hz), 122.58, 135.87, 140.57, 148.957 and 149.087 ($^{3}J_{CF}$=13.0 Hz), 153.22 (2C), 157.900 and 160.294 ($^{1}J_{C-F}$=239 Hz), 166.87, 189.68. MS (ESI): $[M+1]^+$=346.05. HPLC: t_R=18.52 min.

*5.1.3.12. (2-Amino-6-bromobenzofuran-3-yl)(3,4,5-trimethoxyphenyl)methanone (**4k**).* The crude residue purified by flash chromatography, using EtOAc:petroleum ether 1:1 (v:v) for elution, furnished **4k** as a yellow solid. Yield: 78% (Method A), 47% (Method B), mp 170-172 °C. ^{1}H-NMR (DMSO-*d*$_6$) δ: 3.75 (s, 3H), 3.77 (s, 6H), 6.76 (d, J=8.4 Hz, 1H), 6.90 (s, 2H), 7.21 (dd, J=8.4 and 2.0 Hz, 1H), 7.64 (d, J=2.0 Hz, 1H), 8.66 (bs, 2H). ^{13}C-NMR (DMSO-*d*$_6$) δ: 55.86 (2C), 60.13, 91.48, 104.49 (2C), 112.62, 113.06, 119.22, 126.02, 126.34,

136.03, 139.34, 148.64, 152.66 (2C), 166.77, 187.46. MS (ESI): $[M]^+$=405.92, $[M+2]^+$=408.25. HPLC: t_R=20.65 min.

*5.1.3.13. (2-Amino-6-methylbenzofuran-3-yl)(3,4,5-trimethoxyphenyl)methanone (**4l**).* The crude residue purified by flash chromatography, using EtOAc:petroleum ether 1:1 (v:v) for elution, furnished **4l** as a yellow solid. Yield: 73% (Method A), 39% (Method B), mp 137-139 °C. ^{1}H-NMR (DMSO-d_6) δ: 2.28 (s, 3H), 3.74 (s, 3H), 3.75 (s, 6H), 6.72 (d, J=8.0 Hz, 1H), 6.85 (dd, J=8.0 and 0.8 Hz, 1H), 6.89 (s, 2H), 7.15 (d, J=0.8 Hz, 1H), 8.49 (bs, 2H). ^{13}C-NMR (DMSO-d_6) δ: 20.71, 55.82 (2C), 60.12, 91.80, 104.53 (2C), 110.29, 117.74, 123.65, 124.19, 130.83, 136.35, 139.15, 148.64, 152.56 (2C), 166.70, 187.33. MS (ESI): $[M+1]^+$=342.20. HPLC: t_R=18.72 min.

*5.1.3.14. (2-Amino-5-nitrobenzofuran-3-yl)(3,4,5-trimethoxyphenyl)methanone (**7a**).* The crude residue purified by flash chromatography, using EtOAc:petroleum ether 8:2 (v:v) for elution, furnished **7a** as a brown solid. Yield; 68% (Method A), 47% (Method B), mp 95-97 °C. ^{1}H-NMR (DMSO-d_6) δ: 3.78 (s, 3H), 3.79 (s, 6H), 6.98 (s, 2H), 7.62 (d, J=8.2 Hz, 1H), 7.69 (d, J=2.4 Hz, 1H), 8.00 (dd, J=8.2 and 2.4 Hz, 1H), 8.88 (bs, 2H). MS (ESI): $[M+1]^+$=373.27.

*5.1.4. (2-Amino-6-hydroxybenzofuran-3-yl)(3,4,5-trimethoxyphenyl)methanone (**4m**).* (2-Amino-6-(benzyloxy)benzofuran-3-yl)(3,4,5-trimethoxyphenyl)methanone **4i** (0.12 g, 0.28 mmol) was dissolved in a mixture of methanol (25 mL) and ethanol (25 mL) and passed through a H-Cube Pro flow reactor using a 10% Pd/C 70 mm Catcart at 40 bar and 60 °C. Once the reaction was complete, the reaction mixture was concentrated. The final compound was obtained as a yellow solid. Yield 78%, mp 87-89 °C. ^{1}H-NMR (DMSO-d_6) δ: 3.75 (s, 3H), 3.77 (s, 6H), 6.52 (dd, J=8.4 and 1.6 Hz, 1H), 6.66 (d, J=8.4 Hz, 1H), 6.74 (d, J=1.6 Hz, 1H), 6.90 (s, 2H), 8.42 (bs, 2H), 9.36 (bs, 1H). ^{13}C-NMR (DMSO-d_6) δ: 55.81 (2C), 60.08,

91.72, 97.72, 104.47 (2C), 110.99, 118.00, 118.26, 136.46, 139.37, 149.15, 152.53 (2C), 153.06, 166.50, 186.93. MS (ESI): $[M+1]^+$=344.18. HPLC: t_R=14.50 min.

*5.1.5. (2,5-Diaminobenzofuran-3-yl)(3,4,5-trimethoxyphenyl)methanone (**4n**).* To a stirred suspension of (2-amino-5-nitrobenzofuran-3-yl)(3,4,5-trimethoxyphenyl)methanone **7a** (220 mg, 0.59 mmol) in EtOH (10 ml) was added iron powder (230 mg, 4.13 mmol, 7 equiv.) and a solution of ammonium chloride (126 mg, 2.3 mmol, 4 equiv.) in water (1 mL). The reaction mixture was heated under reflux for 1 h, cooled to room temperature, and filtered through Celite. The filter cake was rinsed with dichloromethane (20 mL) and the filtrate washed with water (5 mL) and brine (5 mL) and dried over Na_2SO_4. The solvent was removed under reduced pressure. The crude residue was purified by flash chromatography, using EtOAc:petroleum ether 6:4 (v:v) for elution, and furnished **4n** as an orange solid. Yield 45%, mp 168-170 °C. ^{1}H-NMR (DMSO-d_6) δ: 3.76 (s, 3H), 3.78 (s, 6H), 4.82 (bs, 2H), 6.20 (dd, J=8.4 and 2.4 Hz, 1H), 6.26 (d, J=2.4 Hz, 1H), 6.93 (s, 2H), 6.96 (d, J=8.4 Hz, 1H), 8.41 (bs, 2H). ^{13}C-NMR (DMSO-d_6) δ: 55.79 (2C), 60.08, 92.38, 103.49, 104.78 (2C), 107.74, 109.59, 126.60, 136.12, 139.30, 145.05, 152.46 (2C), 154.09, 167.22, 187.30. MS (ESI): $[M+1]^+$=343.22. HPLC: t_R=12.00 min.

5.2. Biological assays and computational studies.

5.2.1. Cytotoxicity assays.

The cell lines and culture media used were described previously, as were the cell culture methodologies [27]. The 10 mM compound stock solutions were prepared with DMSO, and the DMSO concentration in cytotoxicity and all cell-based assays was always ≤ 0.25%.

Peripheral blood lymphocytes (PBL) from healthy donors were obtained from human peripheral blood (leukocyte rich plasma-buffy coats) from healthy volunteers using the Lymphoprep (Fresenius KABI Norge AS) gradient density centrifugation.

Buffy coats were obtained from the Blood Transfusion Service, Azienda Ospedaliera of Padova and provided at this institution for research purposes. Therefore, no additional informed consent was needed. In addition, buffy coats were provided without identifiers. The experimental procedures were carried out in strict accordance with approved guidelines.

Normal human astrocytes (NHA) were purchased from Lonza (Lonza Inc, CC-2565) and cultured according to the supplier's instructions.

5.2.2. Effects on tubulin polymerization and on colchicine binding to tubulin.

To evaluate the effects of the compounds on tubulin assembly *in vitro* [39], varying concentrations of compounds were preincubated with 10 μM bovine brain tubulin in glutamate buffer at 30 ˚C and then cooled to 0 ˚C. After addition of 0.4 mM GTP (final concentration), the mixtures were transferred to 0 °C cuvettes in a recording spectrophotometer and warmed to 30 °C. Tubulin assembly was followed turbidimetrically at 350 nm. The IC_{50} was defined as the compound concentration that inhibited the extent of assembly by 50% after a 20 min incubation. The ability of the test compounds to inhibit colchicine binding to tubulin was measured as described [40], except that the reaction mixtures contained 0.5 μM tubulin, 5 μM [^{3}H]colchicine and 5 μM or 0.5 μM test compound.

5.2.3. Molecular modeling.

All molecular docking studies were performed on a Viglen Genie Intel®Core™ i7-3770 vPro CPU@ 3.40 GHz x 8 running Ubuntu 184.04. Molecular Operating Environment (MOE) 2019.10 [60] and Maestro (Schrödinger Release 2019-3) [41] were used as molecular modeling software. The tubulin structure was downloaded from the PDB data bank (http://www.rcsb.org/; PDB code 4O2B). The protein was preprocessed using the Schrödinger Protein Preparation Wizard by assigning bond orders, adding hydrogens and performing a restrained energy minimization of the added hydrogens using the OPLS_2005 force field.

Ligand structures were built with MOE and then prepared using the Maestro LigPrep tool by energy minimizing the structures (OPLS_2005 force filed), generating possible ionization states at pH 7±2, and generating tautomers and low-energy ring conformers. After isolating a tubulin dimer structure, a 12 Å docking grid (inner-box 10 Å and outer-box 22 Å) was prepared using as centroid the co-crystallized colchicine. Molecular docking studies were performed using Glide SP precision keeping the default parameters and setting 5 as number of output poses per input ligand to include in the solution. The output database was saved as a mol2 file. The docking results were visually inspected for their ability to bind the active site.

5.2.4 Immunofluorescence analysis.

For immunofluorescence imaging, cells were fixed in cold 4% formaldehyde for 15 min, rinsed and stained with anti-β-tubulin antibody (Sigma-Aldrich S.r.l., Milan, IT) for 2 h at room temperature. After incubation with primary antibody, cells were washed and labeled with species specific secondary antibody conjugated with Alexa 488 dye (Molecular Probes, Carlsbad, CA). Cells were counterstained with DAPI (Sigma-Aldrich, St. Louis, MO). Finally, images were obtained by using a Zeiss confocal microscope LSM800.

5.2.5. Cell cycle analysis.

HeLa cells were treated with the test compounds for 24 h. Cells were harvested by centrifugation and fixed with 70% (v/v) cold ethanol. Cells were lysed with 0.1% (v/v) Triton X-100 containing RNase A and stained with PI. A Beckman Coulter Cytomics FC500 instrument and MultiCycle for Windows software from Phoenix Flow Systems were used to analyze the cells.

5.2.6. Measurement of apoptosis by flow cytometry.

The cells were treated with the test compounds and after different times stained with both PI, to stain DNA, and annexin V-fluorescein isothiocyanate, to stain membrane PS exposed on

the cell surface, following the instructions of the manufacturer (Roche Diagnostics) of the Annexin-V-Fluos reagent.

5.2.7. Measurement of mitochondrial membrane potential and reactive oxygen species. Mitochondrial potential was measured in HeLa cells by flow cytometry as previously described [29], using the fluorescent dye JC-1 (Molecular Probes).

5.2.8. Evaluation of cellular protein expression.

HeLa cells were exposed for various times to **4f**, and the cells were harvested by centrifugation and washed twice in 0 °C phosphate-buffered saline (PBS). Cells were lysed with 0.1% (v/v) Triton X-100 containing RNase A at 0 °C, and supernatants were obtained by centrifuging the lysed cells at 15,000 x g for 10 min at 4 °C. The protein content of the solutions was measured, and 10 μg of protein from each sample was subjected to sodium dodecyl sulfate-polyacrylamide gel electrophoresis. Proteins were transferred by electroblotting to a poly(vinylidene difluoride) Hybond-P membrane from GE Healthcare. The membranes were treated with 5% bovine serum albumin in PBS containing 0.1% Tween 20 overnight at 4 °C. The membranes were then exposed for 2 h at room temperature to primary antibodies directed against cyclin B, BubR1, MAD-2, PARP, caspase-9, Mcl-1 (all from Cell Signaling), Bcl-2 or β-actin (Santa Cruz; to verify equal protein loading) and subsequently for 1 h to peroxidase-labeled secondary antibodies. The membranes were visualized using ECL Select (GE Healthcare), and images were acquired using a Uvitec-Alliance imaging system.

5.2.9. Evaluation of antivascular activity in vitro.

HUVECs were prepared as previously described [57, 58]. The adherent cells were maintained in M200 medium supplemented with Low Serum Growth Supplement, containing fetal bovine serum, hydrocortisone, hEGF, bFGF, heparin and gentamycin/amphotericin B (Life

Technologies, Monza, Italy). Once confluent, the cells were detached with a trypsin–EDTA solution and used in experiments from the first to the sixth passage. Matrigel matrix (Basement Membrane Matrix, BD Biosciences, Italy) was kept at 4 °C for 3 h, when 230 µL of Matrigel solution was added to each well of a 24-well plate. After gelling at 37 °C for 30 min, gels were overlaid with 500 µL of medium containing 6 x 10^4 HUVECs. The cells were incubated over Matrigel for 6 h to allow capillary tubes to form. Different concentrations of test compound were added to the cultures and incubated for different times, and the disappearance of existing vasculature was monitored and photographed (five fields for each well: the four quadrants and the center) at a 10x magnification. Phase contrast images were recorded using a digital camera and saved as TIFF files. Image analysis was carried out using ImageJ image analysis software, and the following dimensional parameters (percent area covered by HUVECs and total length of HUVECs network per field) and topological parameters (number of meshes and branching points per field) were estimated [57, 58].

5.2.10. In vivo evaluation of anti-tumor activity.

Animal experiments were approved by the local animal ethics committee (OPBA, Organismo Preposto al Benessere degli Animali, Università degli Studi di Brescia, Italy) and were performed in accordance with national guidelines and regulations. Procedures involving animals and their care conformed with institutional guidelines that comply with national and international laws and policies (EEC Council Directive 86/609, OJ L 358, 12 December 1987) and with "ARRIVE" guidelines (Animals in Research Reporting In Vivo Experiments). Seven-week-old C57BL/6 female mice were orthotopically injected into the mammary fat pad with 4 × 10^5 E0771 mammary carcinoma cells. When tumors were palpable, mice were randomized to control and treated groups. Treatment was performed every other day by intraperitoneal injection of **4f** (15 or 5 mg/kg), CA-4P (30 mg/kg) or vehicle (DMSO) in a 100 µL final volume. Tumors were measured using a caliper: tumor volume V (mm^3) was

calculated according to the formula $V=(D \times d^2)/2$, where D and d are the major and minor perpendicular tumor diameters in mm, respectively. Tumor volume data were analyzed with a two-way analysis of variance, and individual group comparisons were evaluated by the Bonferroni correction.

5.2.11. Statistical analysis.

Graphs and statistical analyses were performed using GraphPad Prism software (GraphPad, La Jolla, CA, USA). All data in graphs represented the mean of at least three independent experiments ± SEM. Statistical significance was determined using Student's t-test or ANOVA (one- or two-way) depending on the type of data. Asterisks indicate a significant difference between the treated and the control group, unless otherwise specified. * $p < 0.05$, ** $p < 0.01$, *** $p < 0.001$, **** $p < 0.0001$.

Author Contributions. The manuscript was written through contributions of all authors.

Acknowledgment. The authors would like to thank Dr. Alberto Casolari and Dr. Erika Marzola for excellent technical assistance. R.R. and S.M. acknowledge the support of the Italian Ministero dell'Istruzione, Università e della Ricerca - Italy (PRIN 2017, Prot. No. 2017E84AA4_002). S.F. was supported by the Sêr Cymru II programme which is part-funded by Cardiff University and the European Regional Development Fund through the Welsh Government.

Disclaimer. This research was supported in part by the Developmental Therapeutics Program in the Division of Cancer Treatment and Diagnosis of the National Cancer Institute, which includes federal funds under Contract No. HHSN261200800001E. The content of this publication does not necessarily reflect the views or policies of the Department of Health and

Human Services, nor does mention of trade names, commercial products, or organizations imply endorsement by the U.S. Government.

Abbreviations. Abbreviations. CA-4, combretastatin A-4; CA-4P, combretastatin A-4 disodium phosphate; CH_3CN, acetonitrile, *p*-TSA, *p*-toluensulfonic acid; CFL, compact fluorescent lamp; 10% Pd/C, 10% palladium on activated charcoal; DMSO, dimethyl sulfoxide; ESI, electrospray ionization; FITC, fluorescein isothiocyanate; HUVECs, human umbilical vein endothelial cells; JC-1, 5,5',6,6'-tetrachloro-1,1',3,3'-tetraethylbenzimidazolcarbocyanine; NHA, normal human astrocytes; PHA, phytohematoagglutinin; PARP, Poly (ADP-ribose) polymerase; PBS, phosphate-buffered saline; PI, propidium iodide; PBL, peripheral blood lymphocytes; PS, phospholipid phosphatidylserine; SAC, spindle assembly checkpoint.

Supporting information available. ^{1}H-NMR and ^{13}C-NMR spectra of compounds **3c, 7a** and **4a-n**. HPLC traces for compounds **3c** and **4a-n**. Supplementary data associated with this article can be found in the online version.

References.

[1] A. Akhmanova, M.O. Steinmetz. Control of microtubule organization and dynamics: two ends in the limelight. Nat. Rev. Mol. Cell. Biol. 16 (2015) 711-726.

[2] G.J. Brouhard, L.M. Rice. The contribution of αβ-tubulin curvature to microtubule dynamics. J. Cell Biol. 207 (2014) 323-334.

[3] C. Janke. The tubulin code: molecular components, readout mechanisms, and functions. J. Cell Biol. 206 (2014) 461-472.

[4] C.H.S. Aylett, J. Löwe, L.A. Amos. New insights into the mechanisms of cytomotive actin and tubulin filaments. In *International Review of Cell and Molecular Biology;* K.W. Jeon, Ed.; Academic Press: Burlington, 292 (2011), 1-71.

[5] N.G. Vindya, N. Sharma, M. Yadav, K.R. Ethiraj. Tubulins-the target for anticancer therapy. Curr. Top. Med. Chem. 15 (2015) 73-82.

[6] R.J. van Vuuren, M.H. Visagie, A.E. Theron, A.M. Joubert. Antimitotic drugs in the treatment of cancer. Cancer Chemother. Pharmacol. 76 (2015) 1101-1112.

[7] Y.M. Liu, H.L. Chen, H.Y. Lee, J.P. Liou. Tubulin inhibitors: a patent review. Expert Opin. Ther. Pat. 24 (2014) 69-88.

[8] E. Porcù, R. Bortolozzi, G. Basso, G. Viola. Recent advances on vascular disrupting agents. Future Med. Chem. 6 (2014) 1485-1498.

[9] M.J. Perez-Perez, E.M. Priego, O. Bueno, M.S. Martins, M.D. Canela, S. Liekens. Blocking blood flow to solid tumors by destabilizing tubulin: an approach to targeting tumor growth, J. Med. Chem. 59 (2016) 8685-8711.

[10] L.M. Greene, M.J. Meegan, D.M. Zisterer. Combretastatins: more than just vascular targeting agents? J. Pharmacol. Exp. Ther. 355 (2015) 212-227.

[11] G.R. Pettit, S.B. Singh, E. Hamel, C.M. Lin, D.S. Alberts, D. Garcia-Kendall. Isolation and structure of the strong cell growth and tubulin inhibitor combretastatin A-4. Experentia 45 (1989) 209-211.

[12] C.M. Lin, H.H. Ho, G.R. Pettit, E. Hamel. Antimitotic natural products combretastatin A-4 and combretastatin A-2: studies on the mechanism of their inhibition of the binding of colchicine to tubulin. Biochemistry 28 (1989) 6984-6991.

[13] K.G. Pinney, C. Jelinek, K. Edvardsen, D.J. Chaplin, G.R. Pettit. The discovery and development of the combretastatins. In *Antitumor Agents from Natural Products*; D. Kingston, D. Newman, G. Cragg, Eds.; CRC Press: Boca Raton, FL, 2005; 23-46.

[14] P. Nathan, M. Zweifel, A.R. Padhani, D.-M. Koh, M. Ng, D.J. Collins, A. Harris, C. Carden, J. Smythe, N. Fisher, N.J. Taylor, J.J. Stirling, S.-P. Lu, M.O. Leach, G.J.S Rustin, I. Judson. Phase I trial of combretastatin A4 phosphate (CA-4P) in combination with bevacizumab in patients with advanced cancer. Clin. Cancer Res. 18 (2012) 3428-3439.

[15] Q.-S. Ng, H. Mandeville, V. Goh, R. Alonzi, J. Milner, D. Carnell, K. Meer, A.R. Padhani, M.I. Saunders, P.J. Hoskin. Phase Ib trial of radiotherapy in combination with combretastatin-A4-phosphate in patients with non-small-cell lung cancer, prostate adenocarcinoma, and squamous cell carcinoma of the head and neck. Ann. Oncol. 23 (2012) 231-237.

[16] R. Bahleda, C. Sessa, G. Del Conte, L. Gianni, G. Capri, A. Varga, C. Oprea, B. Daglish, M. Hospitel, J.C. Soria. Phase I clinical and pharmacokinetic study of ombrabulin (AVE8062) combined with cisplatin/docetaxel or carboplatin/paclitaxel in patients with advanced solid tumors. Invest. New Drugs 2014, 32, 1188-1196.

[17] A. Delmonte, C. Sessa. AVE8062: a new combretastatin derivative vascular disrupting agents. Exp. Opin. Invest. Drugs 18 (2009) 18, 1541-1548.

[18] M.M. Mita, L. Sargsyan, A.C. Mita, M. Spear. Vascular disrupting agents in oncology. Expert. Opin. Invest. Drugs 22 (2013) 317-328.

[19] Y.T. Ji, Y.N. Liu, Z.P. Liu. Tubulin colchicine binding site inhibitors as vascular disrupting agents in clinical developments. Curr. Med. Chem. 22 (2015) 1348-1360.

[20] S.N.A. Bukhari, G.B. Kumar, H.M. Revankar, H.L. Qin. Development of combretastatins as potent tubulin polymerization inhibitors. Bioorg. Chem. 72 (2017) 130-147.

[21] Z.S. Seddigi, M.S. Malik, A.P. Saraswati, S.A. Ahmed, A.O. Babalghith, H.A. Lamfon, A. Kamal. Recent advances in combretastatin based derivatives and prodrugs as antimitotic agents. Med. Chem. Commun. 8 (2017) 1592-1603.

[22] E.C. McLoughlin, N.M. O'Boyle. Colchicine-binding site inhibitors from chemistry to clinic: a review. Pharmaceuticals. 13 (2020) 8.

[23] A. Kamal, N.V.S. Reddy, V.L. Nayak, V.S. Reddy, B. Prasad, V.D. Nimbarte, V. Srinivasulu, M.V.P.S. Vishunuvardhan, C.S. Reddy. Synthesis and biological evaluation of benzo[*b*]furans as inhibitors of tubulin polymerization and inducers of apoptosis. ChemMedChem 9 (2014), 117-128.

[24] B. Tréguier, E. Rasolofonjatovo, A. Hamze, O. Provot, J. Wdzieczak-Bakala, J. Dubois, J.-D. Brion, M. Alami. Synthesis of 2-(1-phenylvinyl)benzofurans and 2-(1-phenylvinyl)indoles as antimitotic agents by a tandem palladium-assisted coupling-cyclization reaction between 1-phenylvinyl iodides and *ortho*-substituted arylalkynes. Eur. J. Org. Chem. 25 (2011) 4868-4876.

[25] Y. P. Quan, L. P. Cheng, T. C. Wang, W. Pang, F. H. Wu, J. W. Huang. Molecular modeling study, synthesis and biological evaluation of combretastatin A-4 analogues as anticancer agents and tubulin inhibitors. Med. Chem. Commun. 9 (2018) 316-327.

[26] R. Romagnoli, P.G. Baraldi, T. Sarkar, M.D. Carrion, O. Cruz-Lopez, C. Lopez-Cara, M. Tolomeo, S. Grimaudo, A. Di Cristina, M.R. Pipitone, J. Balzarini, R. Gambari, I. Lampronti, R. Saletti, A. Brancale, E. Hamel. Synthesis and biological evaluation of 2-(3',4',5'-trimethoxybenzoyl)-3-*N,N*-dimethylamino benzo[*b*]furan derivatives as inhibitors of tubulin polymerization. Bioorg. Med. Chem. 16 (2008) 8419-8426.

[27] R. Romagnoli, P.G. Baraldi, M. Kimatrai Salvador, F. Prencipe, C. Lopez-Cara, S. Schiaffino Ortega, A. Brancale, E. Hamel, I. Castagliuolo, S. Mitola, R. Ronca, R. Bortolozzi, E. Porcù, G. Basso, G. Viola. Design, synthesis, in vitro and in vivo

anticancer and antiangiogenic activity of novel 3-arylamino benzofuran derivatives targeting the colchicine site on tubulin. J. Med. Chem. 58 (2015) 3209-3222.

[28] R. Romagnoli, P.G. Baraldi, C. Lopez Cara, O. Cruz-Lopez, M.D. Carrion, M. Kimatrai Salvador, J. Bermejo, S. Estévez, F. Estévez , J. Balzarini, A. Brancale, A. Ricci, L. Chen, J. G. Kim, E. Hamel. Synthesis and antitumor molecular mechanism of agents based on amino 2-(3',4',5'-trimethoxybenzoyl)-benzo[*b*]furan: inhibition of tubulin and induction of apoptosis. ChemMedChem 6 (2011) 1841-1853.

[29] B.L. Flynn, E. Hamel, M.K. Jung. One-pot synthesis of benzo[*b*]furan and indole inhibitors of tubulin polymerization. J. Med. Chem. 45 (2002) 2670-2673.

[30] B.L. Flynn, G.S. Gill, D.S. Grobelny, J.H. Chaplin, D. Paul, A.F. Leske, T.C. Lavranos, D.K. Chalmers, S.A. Charman, E. Kostewicz, D.M. Shackleford, J. Morizzi, E. Hamel, M.K. Jung, G. Kremmidiotis. Discovery of 7-hydroxy-6-methoxy-2-methyl-3-(3,4,5-trimethoxybenzoyl)benzo[*b*]furan (BNC 105), a tubulin polymerization inhibitor with potent antiproliferative and tumor vascular disrupting properties. J. Med. Chem. 54 (2011) 6014-6027.

[31] G. Kremmidiotis, A.F. Leske, T.C. Lavranos, D. Beaumont, J. Gasic, A. Hall, M. O'Callaghan, C.A. Matthews, B.L. Flynn. BNC105: a novel tubulin polymerization inhibitor that selectively disrupts tumor vasculature and displays single-agent antitumor efficacy. Mol. Cancer Ther. 9 (2010) 1562-1573.

[32] R. Romagnoli, P.G. Baraldi, M.D. Carrion, C. Lopez Cara, D. Preti, F. Fruttarolo, M.G. Pavani, M. Aghazadeh Tabrizi, M. Tolomeo, S. Grimaudo, C. Di Antonella, J. Balzarini, J.A. Hadfield, A. Brancale, E. Hamel. Synthesis and biological evaluation of 2- and 3-aminobenzo[*b*]thiophene derivatives as antimitotic agents and inhibitors of tubulin polymerization. J. Med. Chem. 50 (2007) 2273-2277.

[33] R. Romagnoli, P.G. Baraldi, T. Sarkar, M.D. Carrion, C. Lopez-Cara, O. Cruz-Lopez, D. Preti, M.A. Tabrizi, M. Tolomeo, S. Grimaudo, A. Di Cristina, N. Zonta, J. Balzarini, A. Brancale, H.P. Hsieh, E. Hamel. Synthesis and biological evaluation of 1-methyl-2-(3',4',5'-trimethoxybenzoyl)-3-amino indoles as a new class of antimitotic agents and tubulin inhibitors. J. Med. Chem. 51 (2008) 1464-1468.

[34] S. Borra, D. Chandrasekhar, S. Khound, R.A. Maurya. Access to 1*a*,6*b*-dihydro-1*H*-benzofuro[2,3-*b*]azirines and benzofuran-2-amines via visible light triggered decomposition of α-azidochalcones. Org. Lett. 19 (2017) 5364−5367.

[35] For the synthesis and characterization of 4-ethoxy-2-hydroxybenzaldehyde (**5f**) see: K. Binnemans, Y.G. Galyametdinov, R. Van Deun, D.W. Bruce, S.R. Collinson, A.P. Polishchuk, I. Bikchantaev, W. Haase, A.V. Prosvirin, L. Tinchurina, I. Litvinov, A. Gubajdullin, A. Rakhmatullin, K. Uytterhoeven, L. Van Meervelt. Rare-earth-containing magnetic liquid crystals. J. Am. Chem. Soc. 122 (2000) 4335-4344.

[36] For the synthesis and characterization of 4-*n*-propoxy-2-hydroxybenzaldehyde (**5g**) see: H.-M. Kuo, Y.-T. Hsu, Y.-W. Wang, G.-H. Lee, C.K. Lai. The π-π interactions enhanced in salicylaldimines and salicylaldazines. Tetrahedron 71 (2015) 7729-7738.

[37] For the synthesis and characterization of 4-methoxy-2,3-dihydroxybenzaldehyde (**5n**) see: S. Han, F.-F. Zhang, H.-Y. Qian, L.-L. Chen, J.-B. Pu, X. Xie, J.-Z. Chen. Design, syntheses, structure-activity relationships and docking studies of coumarin derivatives as novel selective ligands for the CB2 receptor. Eur. J. Med. Chem. 93 (2015) 16-32.

[38] 2-Azido-1-(3,4,5-trimethoxyphenyl)ethanone was synthesized from the corresponding 2-bromo-1-(3,4,5-trimethoxyphenyl)ethanone and sodium azide using the procedure reported in the following article: B. Prasad, V.G. Reddy, N.H. Krishna, N.V.S. Reddy, J.B. Nanubolu, A. Alarifi, A. Kamal. Annulation of 4-hydroxypyrones and α-keto

vinyl azides; A regiospecific approach towards the synthesis of furo[3,2-*c*]pyrone scaffolds under catalyst free condition. Chemistry Select 2 (2017) 8122-8126.

[39] E. Hamel. Evaluation of antimitotic agents by quantitative comparisons of their effects on the polymerization of purified tubulin. Cell Biochem. Biophys. 38 (2003) 1-21.

[40] P. Verdier-Pinard, J.-Y. Lai, H.-D. Yoo, J. Yu, B. Marquez, D.G. Nagle, M. Nambu, J.D. White, J.R. Falck, W.H. Gerwick, B.W. Day, E. Hamel. Structure-activity analysis of the interaction of curacin A, the potent colchicine site antimitotic agent, with tubulin and effects of analogs on the growth of MCF-7 breast cancer cells. Mol. Pharmacol. 53 (1998) 62-76.

[41] Schrödinger Release 2019-3: Maestro, Schrödinger, LLC, New York, NY, 2019.

[42] A. Musacchio. The molecular biology of spindle assembly checkpoint signaling dynamics. Curr. Biol. 25 (2015) 1002-1018.

[43] H.Y. Yamada, G.J. Gorbsky. Spindle checkpoint function and cellular sensitivity to antimitotic drugs. Mol. Cancer Ther. 5 (2006) 2963-2969.

[44] H.J. Choi, M. Fukui, B.T. Zhu. Role of cyclin B1/Cdc2 up-regulation in the development of mitotic prometaphase arrest in human breast cancer cells treated with nocodazole. PLoS One 6 (2011) e24312.

[45] R. Romagnoli, P.G. Baraldi, C. Lopez-Cara, M. Kimatrai Salvador, D. Preti, M. Aghazadeh Tabrizi, J. Balzarini, P. Nussbaumer, A. Brancale, X.-H. Fu, J. Li; S.-Z. Zhang, E. Hamel, R. Bortolozzi, G. Basso, G. Viola. Design, synthesis and biological evaluation of 3,5-disubstituted 2-amino thiophene derivatives as a novel class of antitumor agents. Bioorg. Med. Chem. 22 (2014) 5097-5109.

[46] A. Rovini, A. Savry, D. Braguer, M. Carré. Microtubule-targeted agents: when mitochondria become essential to chemotherapy. Biochim. Biophys. Acta - Bioenerg. 1807 (2011) 679-688.

[47] R. Romagnoli, P.G. Baraldi, M. Salvador Kimatrai, D. Preti, M. Aghazadeh Tabrizi, A. Brancale, X.-H. Fu, J. Li, S.-Z. Zhang, E. Hamel, R. Bortolozzi, E. Porcù, G. Basso, G. Viola. Discovery and optimization of a series of 2-aryl-4-amino-5-(3',4',5'-trimethoxybenzoyl)thiazoles as novel anticancer agents. J. Med. Chem. 55 (2012) 5433-5445.

[48] R. Romagnoli, P.G. Baraldi, M. Kimatrai Salvador, F. Prencipe, V. Bertolasi, M. Cancellieri, A. Brancale, E. Hamel, I. Castagliuolo, F. Consolaro, E. Porcù, G. Basso, G. Viola. Synthesis, antimitotic and antivascular activity of 1-(3',4',5'-trimethoxybenzoyl)-3-arylamino-5-amino-1,2,4-triazoles. J. Med. Chem. 57 (2014) 6795-6808.

[49] E. Lugli, L. Troiano, A. Cossarizza, Polychromatic analysis of mitochondrial membrane potential using JC-1. Curr. Protoc. Cytom. Chapter 7 (2007) Unit7.32.

[50] S. Shalini, L. Dorstyn, S. Dawar, S. Kumar. Old, new and emerging functions of caspases. Cell Death Differ. 22 (2015) 526-539.

[51] P. Li, L. Zhou, T. Zhao, X. Liu, P. Zhang, Y Liu. X. Zheng, Q. Li. Caspase-9: structure, mechanisms and clinical application. Oncotarget 8 (2017) 23996-24008.

[52] C. Soldani, A.I. Scovassi, A.I. Poly(ADP-ribose) polymerase-1 cleavage during apoptosis: an update. Apoptosis. 7 (2002) 321-328.

[53] P.E. Czabotar, G. Lessene, A. Strasser, J.M. Adams. Control of apoptosis by the BCL-2 protein family: implications for physiology and therapy. Nature Rev. Mol. Cell Biol. 15 (2014) 49-63.

[54] J.M. Eichhorn, N. Sakurikar, S.E. Alford, R. Chu, T.C. Chambers. Critical role of anti-apoptotic Bcl-2 protein phosphorylation in mitotic death. Cell Death Dis. 4 (2013) e834.

[55] I.E. Wertz, S. Kusam, C. Lam, T. Okamoto, W. Sandoval, D.J. Anderson, E. Helgason, J.A. Ernst, M. Eby, J. Liu, L.D. Belmont, J.S. Kaminker, K. M. O'Rourke, K. Pujara, P.B. Kohli, A.R. Johnson, M.L. Chiu, J.R. Lill, P.K. Jackson, W.J. Fairbrother, S. Seshagiri, M.J. Ludlam, K.G. Leong, E.C. Dueber, H. Maecker, D.C. Huang, V.M. Dixit. Sensitivity to antitubulin chemotherapeutics is regulated by MCL1 and FBW7. Nature 471 (2011) 110-114.

[56] M.D. Haschka, C. Soratroi, S. Kirschnek, G. Häcker, R. Hilbe, S. Geley, A. Villunger, L.L Fava. The NOXA-MCL1-BIM axis defines lifespan on extended mitotic arrest. Nat. Commun. 6 (2015) 6891.

[57] E. Porcù, G. Viola, R. Bortolozzi, S. Mitola, R. Ronca, M. Presta, L. Persano, R. Romagnoli, P.G. Baraldi, G. Basso. TR-644 a novel potent tubulin binding agent induces impairment of endothelial cells function and inhibits angiogenesis. Angiogenesis 16 (2013), 647-662.

[58] E. Porcù, L. Persano, R. Ronca, S. Mitola, R. Bortolozzi, R. Romagnoli, P. Oliva, G. Basso, G. Viola, The novel antitubulin agent TR-764 strongly reduces tumor vasculature and inhibitis HIF-1α activation. Sci. Rep. 6 (2016), 27886.

[59] R. Ronca, E. Di Salle, A. Giacomini, D. Leali, P. Alessi, D. Coltrini, C. Ravelli, S. Matarazzo, D. Ribatti, W. Vermi, M. Presta. Long pentraxin-3 inhibits epithelial-mesenchymal transition in melanoma cells. Mol. Cancer Ther. 12 (2013) 2760-2771.

[60] ULC, C. C. G. Molecular Operating Environment (MOE), 2019.10, 1010 Sherbooke St. West, Suite #910, Montreal, QC, Canada, H3A 2R7, 2019.

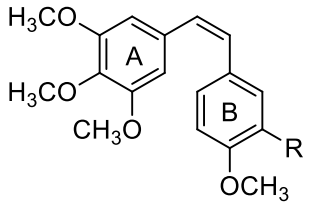

1

R=OH, Combretastatin A-4 (CA-4), **1a**
R=OPO_3Na_2, CA-4P, **1b**
R=NH-Ser, Ombrabulin (AVE8062), **1c**

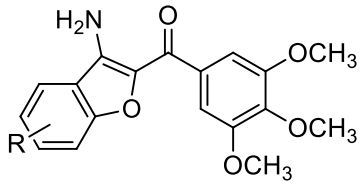

2

R=H or OMe
R=6-OCH_3, **2a**

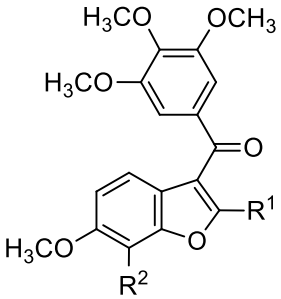

3

R^1=H, Br, CN, CO_2CH_3, alkyl, alkylamine, aryl, heteroaryl
R^2=H or OH
3a, R^1=4'-OMe-3'-OH-C_6H_3, R^2=OH
3b, R^1=CH_3, R^2=OH
3c, R^1=NH_2, R^2=OH

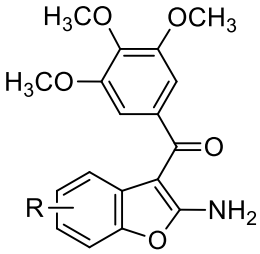

4

R=H, electron-withdrawing (F and Br) or electron-releasing groups such as alkoxy (OCH_3, OC_2H_5, n-OC_3H_7, $OCH_2C_6H_5$), CH_3, OH and NH_2

Figure 1.

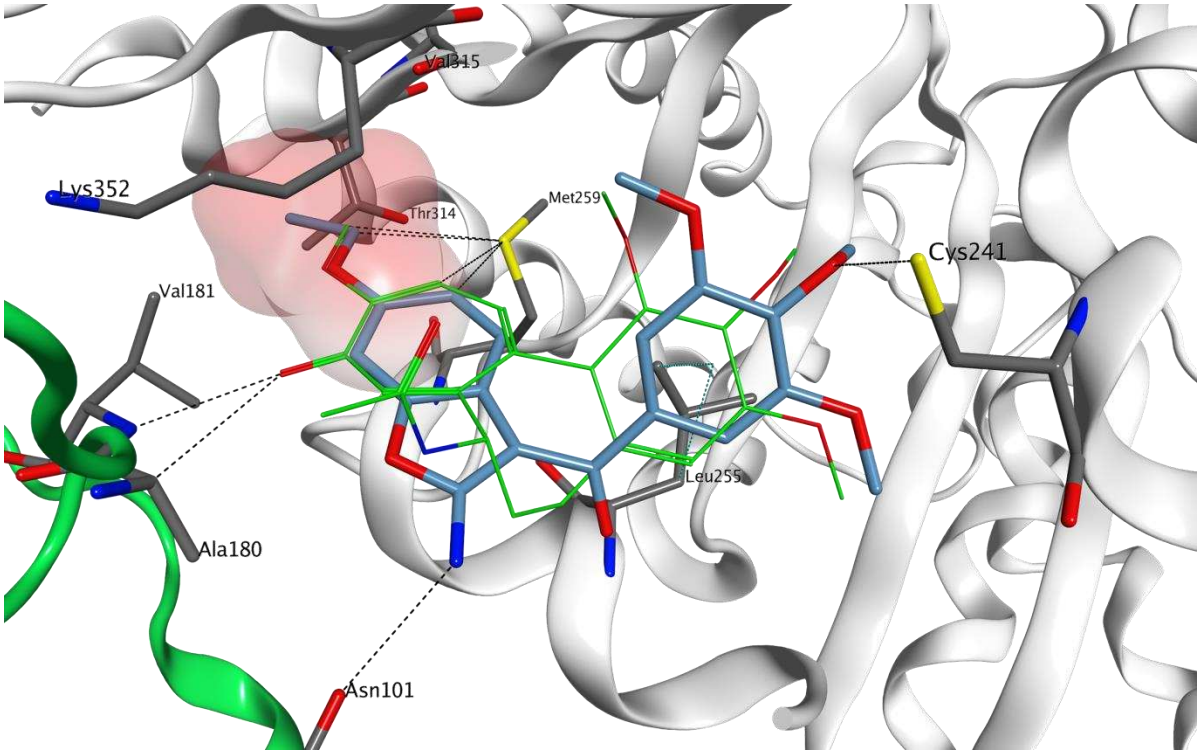
Val315
Lys352
Thr314
Met259
Cys241
Val181
Leu255
Ala180
Asn101

A

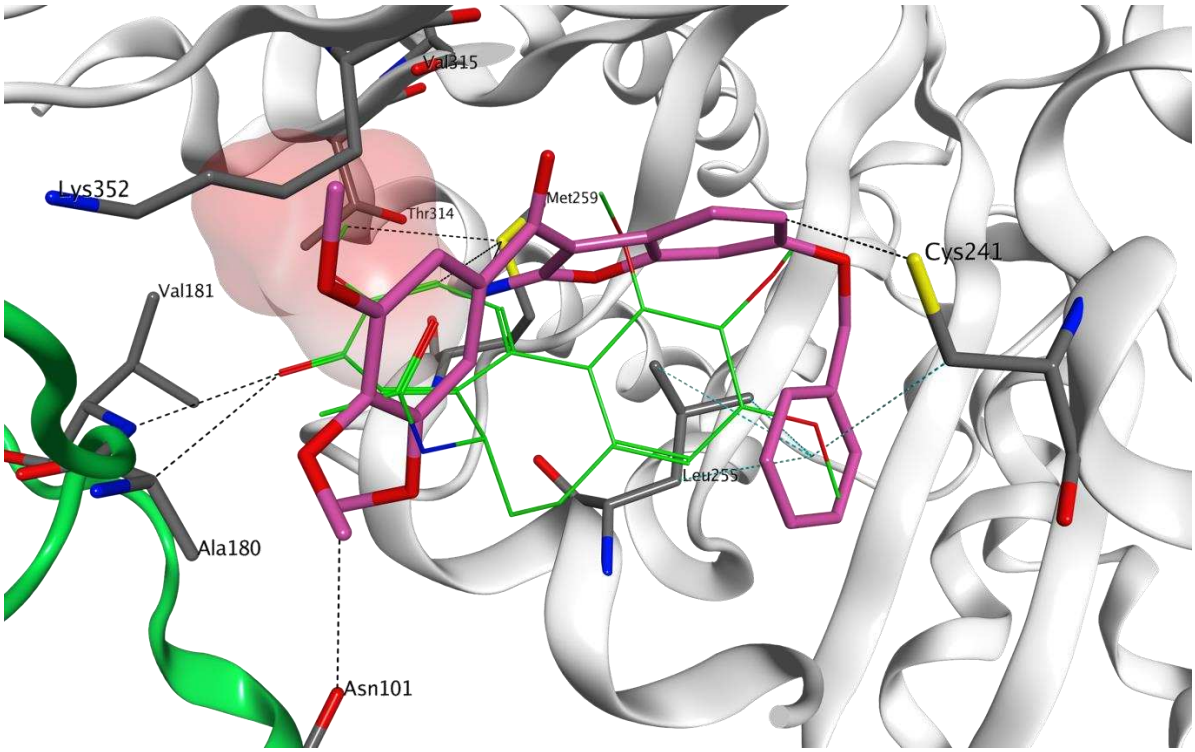
Val315
Lys352
Thr314
Met259
Cys241
Val181
Leu255
Ala180
Asn101

B

Figure 2.

.

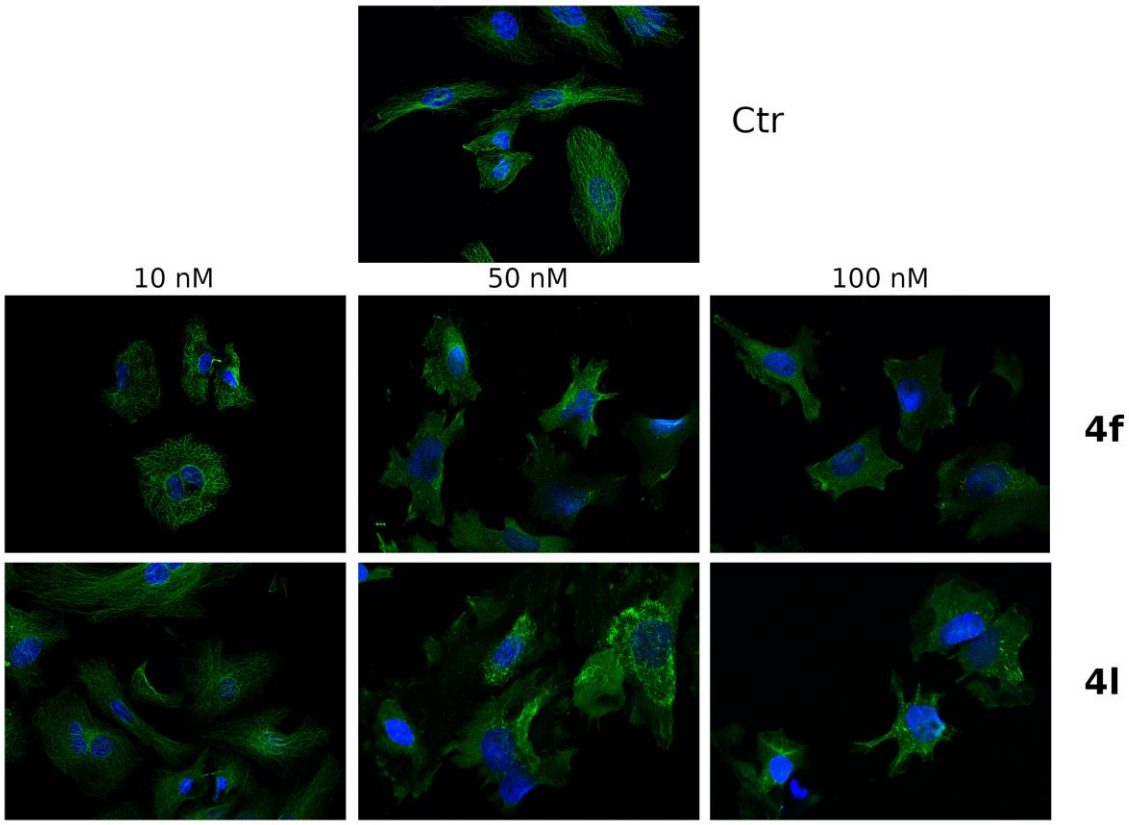

Figure 3

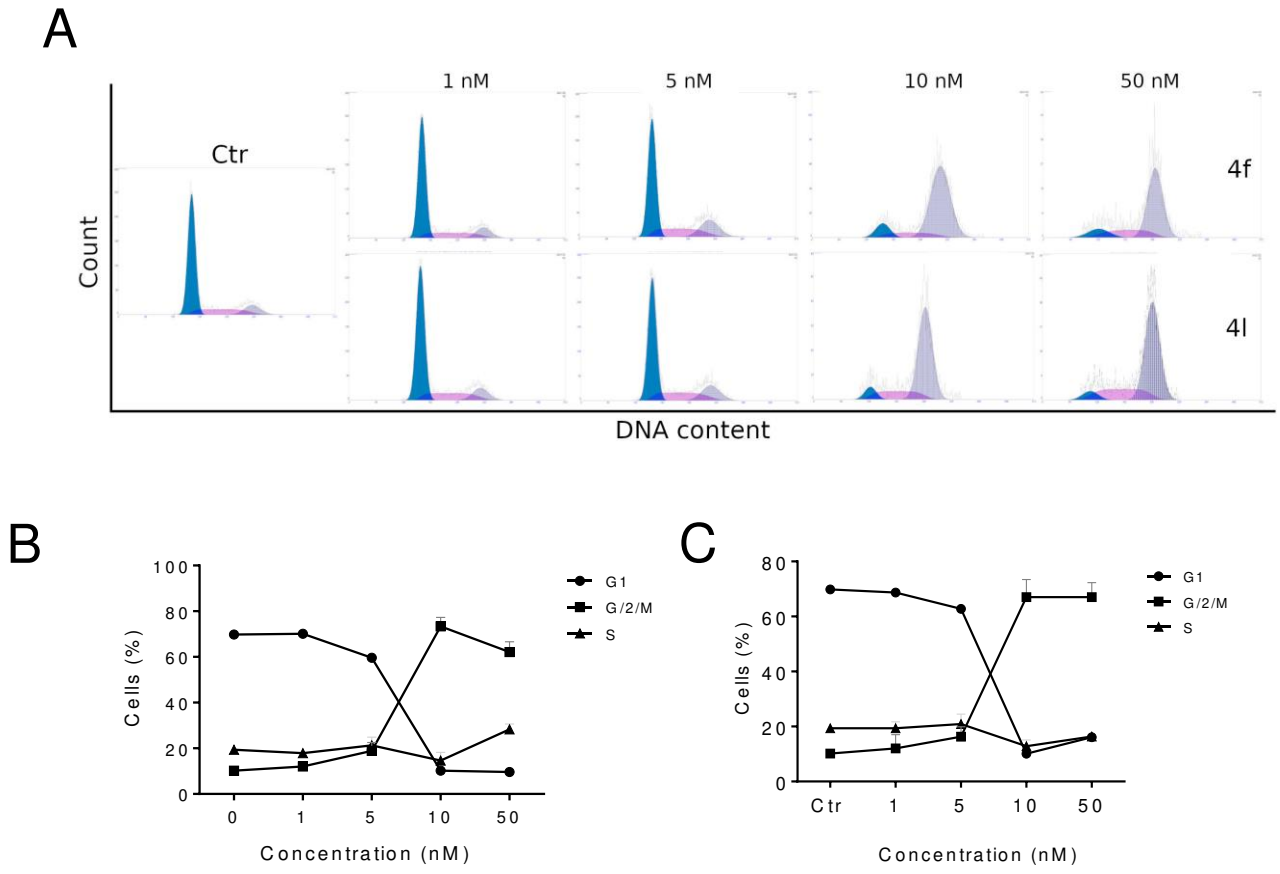
A
1 nM
5 nM
10 nM
50 nM
Ctr
4f
4l
Count
DNA content
B
Cells (%)
Concentration (nM)
G1
G/2/M
S
C
Cells (%)
Ctr
Concentration (nM)
G1
G/2/M
S

Figure 4.

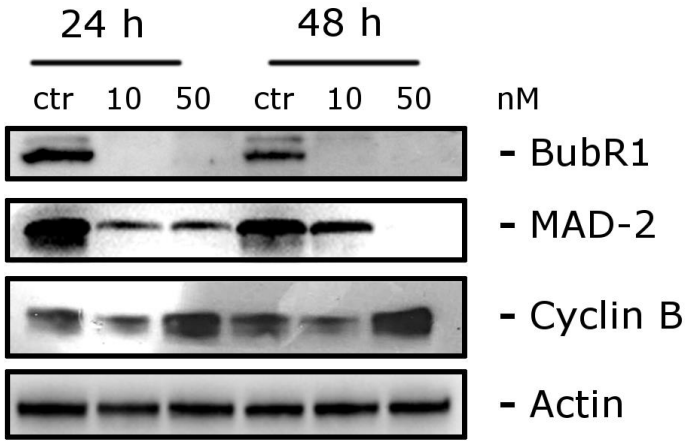

Figure 5.

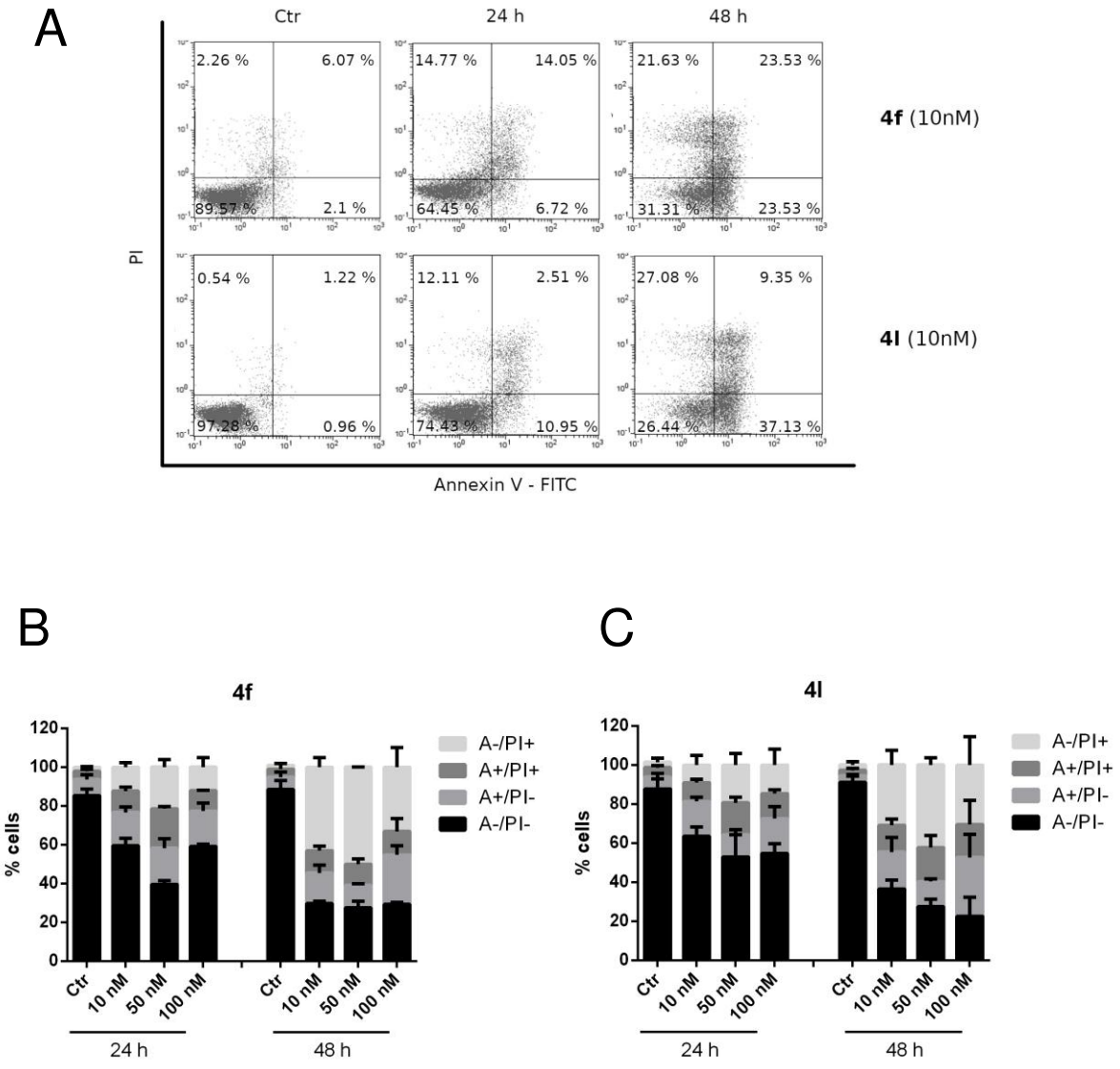
A
Ctr
24 h
48 h
2.26 %
6.07 %
89.57 %
2.1 %
14.77 %
14.05 %
64.45 %
6.72 %
21.63 %
23.53 %
31.31 %
23.53 %
4f (10nM)
0.54 %
1.22 %
97.28 %
0.96 %
12.11 %
2.51 %
74.43 %
10.95 %
27.08 %
9.35 %
26.44 %
37.13 %
4l (10nM)
PI
Annexin V - FITC
B
4f
% cells
A-/PI+
A+/PI+
A+/PI-
A-/PI-
Ctr
10 nM
50 nM
100 nM
24 h
48 h
C
4l

Figure 6.

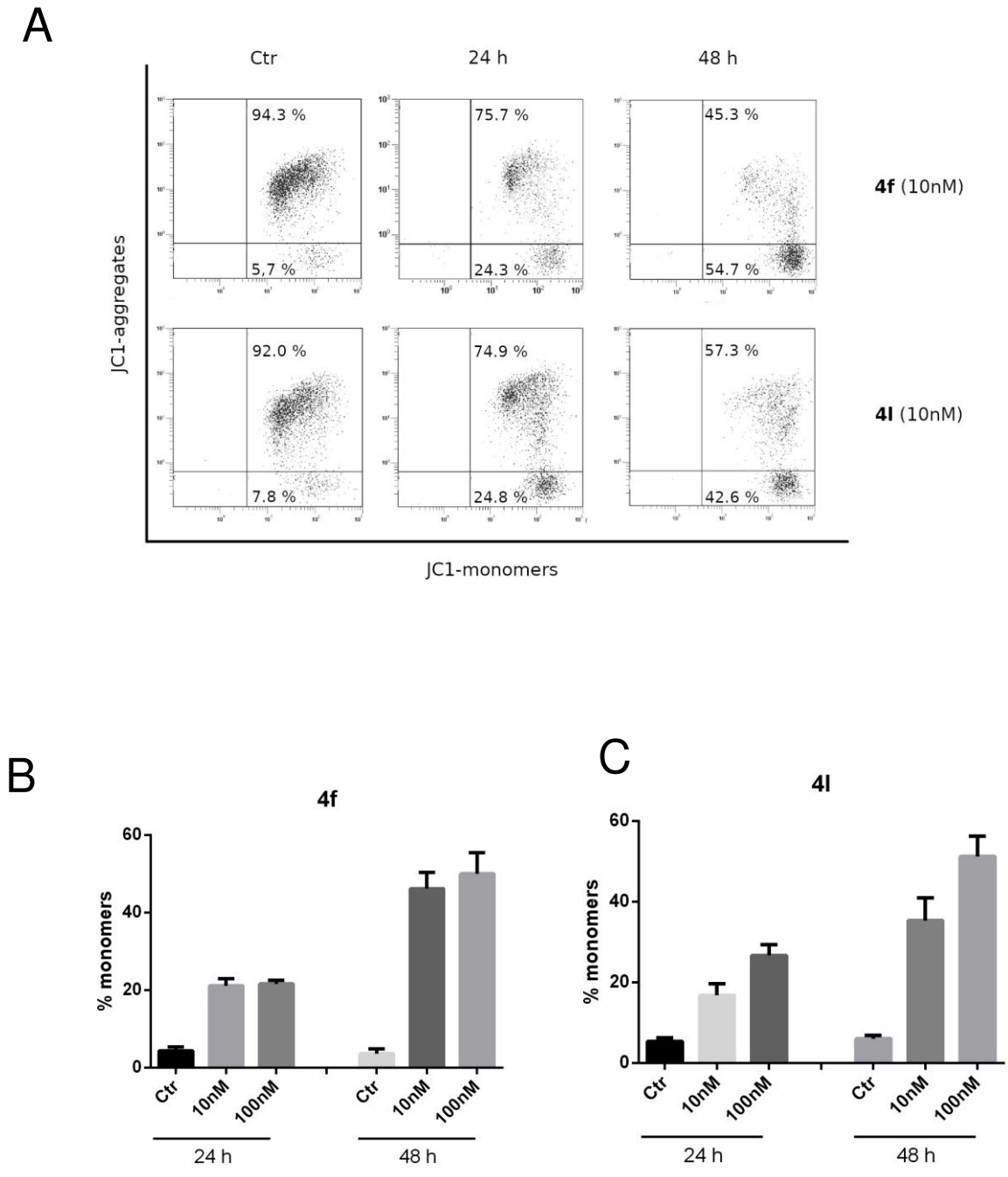
A
Ctr
24 h
48 h
94.3 %
5,7 %
75.7 %
24.3 %
45.3 %
54.7 %
4f (10nM)
92.0 %
7.8 %
74.9 %
24.8 %
57.3 %
42.6 %
4l (10nM)
JC1-aggregates
JC1-monomers
B
4f
% monomers
60
40
20
0
Ctr
10nM
100nM
Ctr
10nM
100nM
24 h
48 h
C
4l
% monomers
60
40
20
0
Ctr
10nM
100nM
Ctr
10nM
100nM
24 h
48 h

Figure 7.

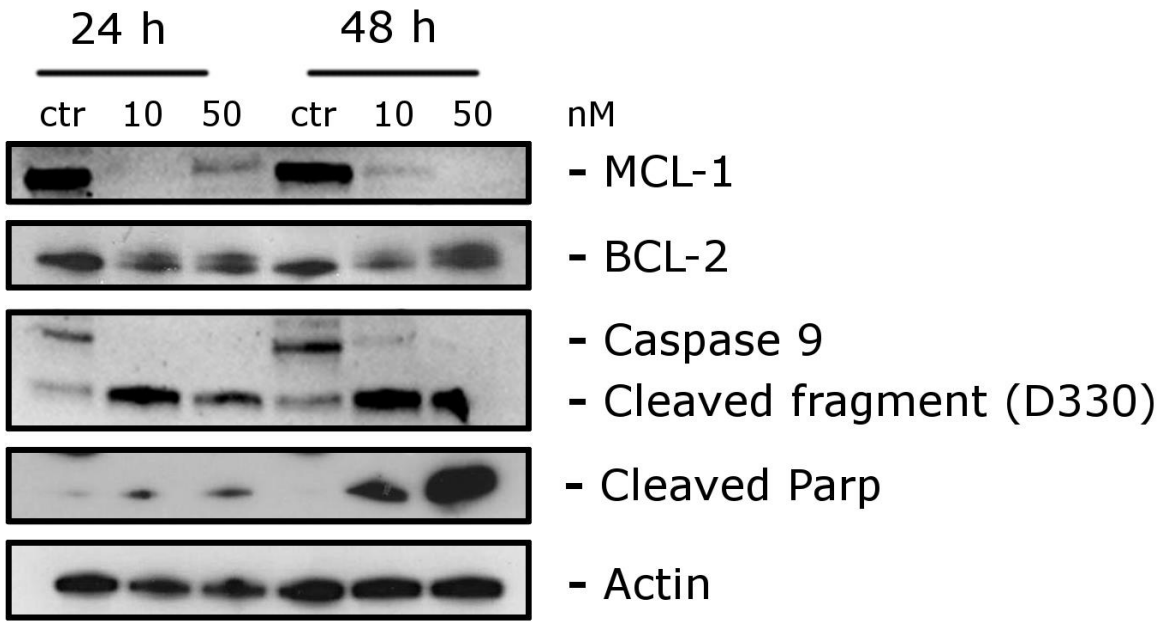
24 h
48 h
ctr 10 50 ctr 10 50
nM
- MCL-1
- BCL-2
- Caspase 9
- Cleaved fragment (D330)
- Cleaved Parp
- Actin

Figure 8.

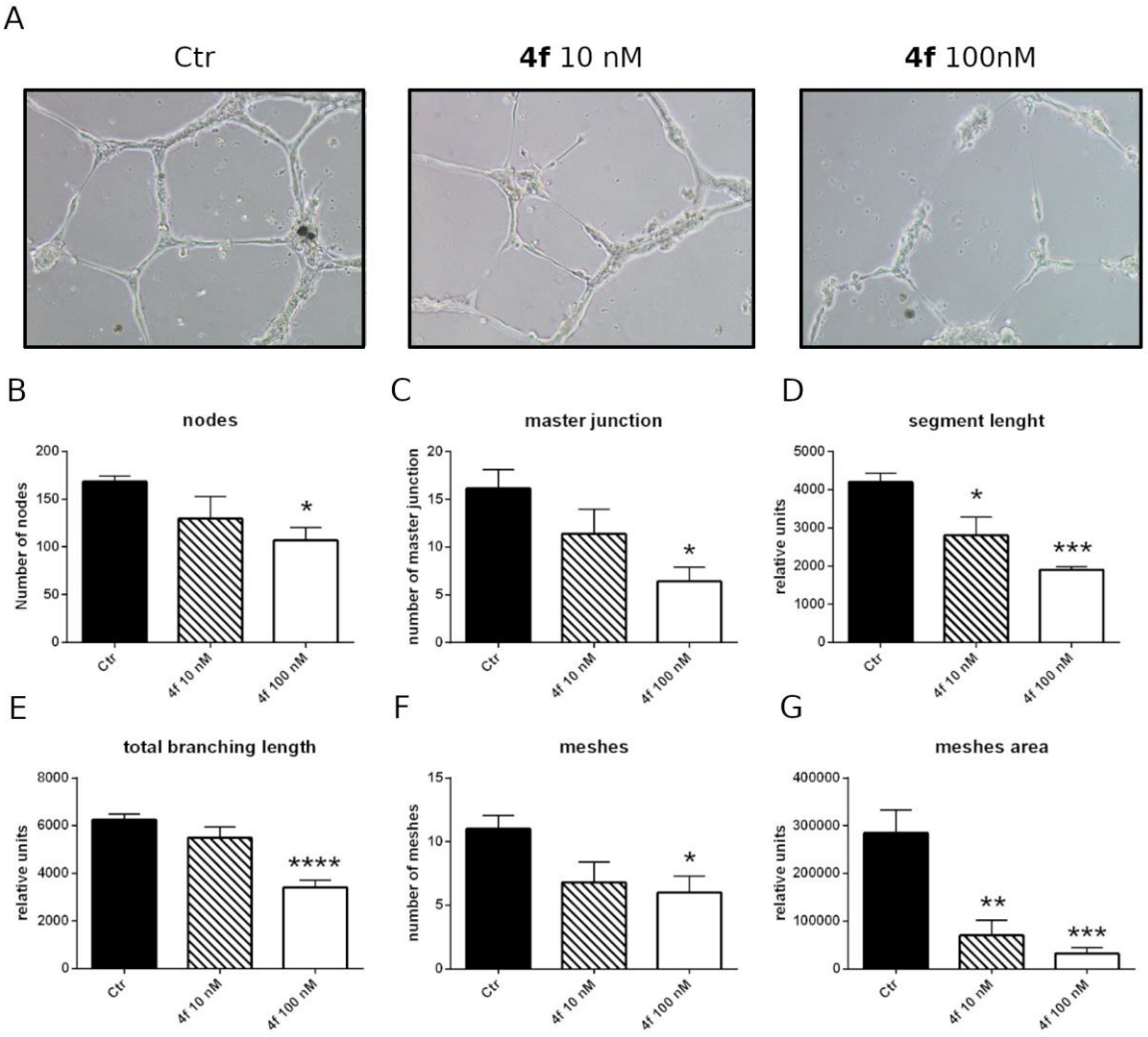
A
Ctr
4f 10 nM
4f 100nM
B
nodes
Number of nodes
C
master junction
number of master junction
D
segment lenght
relative units
E
total branching length
relative units
F
meshes
number of meshes
G
meshes area
relative units
Ctr
4f 10 nM
4f 100 nM

Figure 9.

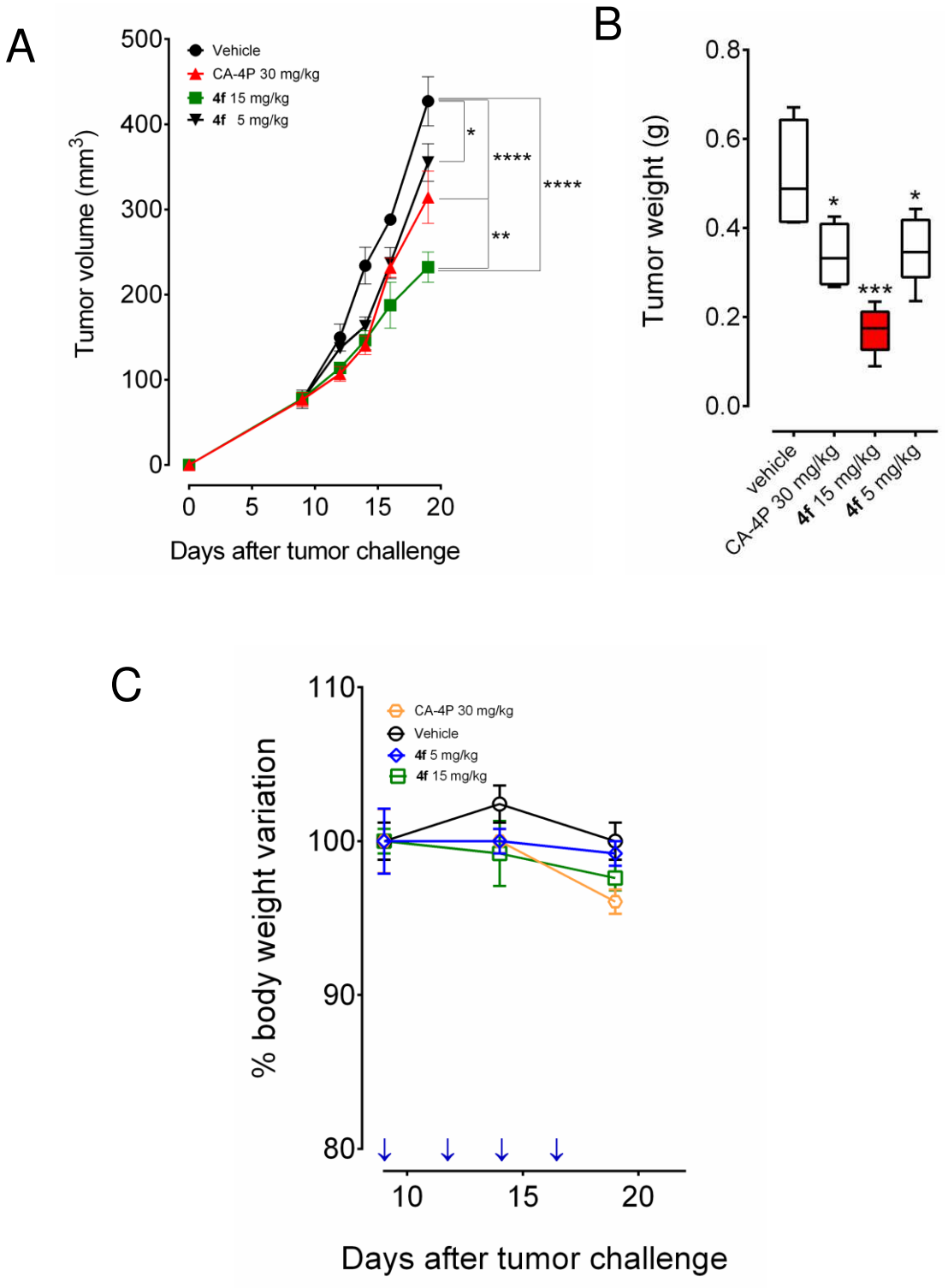
A
Vehicle
CA-4P 30 mg/kg
4f 15 mg/kg
4f 5 mg/kg
Tumor volume (mm3)
Days after tumor challenge
*
****
****
**
B
Tumor weight (g)
vehicle
CA-4P 30 mg/kg
4f 15 mg/kg
4f 5 mg/kg
C
CA-4P 30 mg/kg
Vehicle
4f 5 mg/kg
4f 15 mg/kg
% body weight variation
Days after tumor challenge

Figure 10.